Published in final edited form as:
Prog Nucl Magn Reson Spectrosc. 2011 November ; 59(4): 319–335. doi:10.1016/j.pnmrs.2011.04.002.

In vivo oxygen-17 NMR for imaging brain oxygen metabolism at high field

Xiao-Hong Zhu and **Wei Chen**
Center for Magnetic Resonance Research, Departments of Radiology, University of Minnesota Medical School, 2021 6thSt. SE, Minneapolis, MN 55455

Keywords

In vivo^{17}O NMR; brain; high field; cerebral metabolic rate of oxygen utilization; oxidative metabolism

1. Introduction

The oxygen element is one of the most important components for life on earth because various oxygen containing molecules are present in all levels of biological systems, and oxygen accounts for two thirds of the total human body mass and 90% of the mass of water. However, *in vivo* oxygen-17 (^{17}O) NMR has received very little attention compared to other *in vivo* NMR methodologies, such as ^{1}H, ^{13}C and ^{31}P NMR; even though the ^{17}O NMR signal was first observed in 1951 [1] and utilized since then for many chemical and biochemical applications (see a recent review by Gerothanassis [2, 3] and the cited references therein).

It has been demonstrated that *in vivo* ^{17}O NMR can be used to monitor the uptake or washout of an ^{17}O-labeled exogenous agent (e.g. ^{17}O-labeled water) for studying tissue perfusion [4–7] or for detecting oxygen-containing metabolites in living species [8–10]. Nevertheless, the most valuable and unique capability of *in vivo* ^{17}O NMR is to non-invasively determine the metabolic rate of oxygen in live animals or humans (see [11–13] and references cited therein).

In this review article, we attempt to provide an overview of the methodology background and the present status of *in vivo* ^{17}O MR spectroscopy (MRS)/imaging (MRI) approach for imaging the cerebral metabolic rate of oxygen ($CMRO_2$) and studying the central roles of cerebral oxygen metabolism in brain function. The challenges and potentials of this ^{17}O-MR based $CMRO_2$ imaging method will also be discussed.

*Correspondence Author: Xiao-Hong Zhu, PhD or Wei Chen, PhD, Center for Magnetic Resonance Research, Departments of Radiology and Biomedical Engineering, University of Minnesota, 2021 6th St. SE, Minneapolis, MN 55455, USA, Phone: (612) 625-8814, Fax: (612) 626-2004, zhu@cmrr.umn.edu or wei@cmrr.umn.edu.

2. Background

2.1 Importance of oxygen metabolism in brain function and dysfunction

The brain is a highly aerobic organ; it consumes oxygen and glucose extensively in order to generate chemical energy in the form of the adenosine triphosphate (ATP) molecule. A majority of brain energy is used to support the unceasing electrophysiological activities of neurons responsible for inter-neuron transmission and communication throughout the central nervous system. A coupling between neuronal activity and brain energy exists for a wide range of physiological conditions characterized by the highly dynamic change of neuronal activity. This requires a timely efficient balance between ATP demand and supply, which is regulated by a number of crucial biochemical reactions associated with brain metabolisms and neuroenergetics.

Fig. 1 illustrates the key metabolic processes occurring in various sub-cellular compartments and the associated vascular/hemodynamic events of the brain. Oxygen and glucose as the major fuels for brain metabolism are continuously supplied by the circulating blood flow through the capillary bed. Glucose is transported into brain cells and converted to two pyruvate molecules in the cytosol via glycolysis, which are then converted to acetyl-Co A in the mitochondrion and oxidized via the tricarboxylic acid cycle to generate reducing equivalents of NADH and $FADH_2$. These high energy electron carriers enter the electron transport chain and generate an electrochemical potential gradient across the mitochondrial inner membrane to drive the conversion of adenosine diphosphate (ADP) and inorganic phosphate (Pi) into ATP via oxidative phosphorylation where the electrons are finally transferred to exogenous oxygen and, with the addition of two protons, the final product of water is formed. Under normal physiological conditions with adequate cellular oxygen availability, oxidative phosphorylation comprises ~90% of ATP production [14]. Meanwhile, ATP utilization occurs in the cytosol and results in the reversal conversion of ATP to ADP and Pi with released energy for supporting various neuronal activities.

In general, the brain glucose and oxygen consumptions and ATP production are closely coupled in a functional brain as illustrated by Fig. 1. This coupled metabolic reaction chain can be divided into two parts. One is an open system involving the cerebral metabolisms of glucose (from the food chain) and oxygen (from air), resulting in the final products of water and CO_2 that are washed out into the blood stream. Another one is a close system involving extremely efficient cycling between the ATP generation in the mitochondria and utilization in the cytosol inside the cells. These two systems are integrated and work together to maintain normal brain function.

In comparison with the non-oxidative glycolysis, oxidative phosphorylation produces at least 15 times more ATP molecules. Therefore, brain function relies on the ATP energy and the ATP generation relies heavily on the oxygen metabolism in mitochondria. Abnormalities in brain metabolisms, in particular, related to oxidative phosphorylation have been linked to numerous brain disorders and neurodegenerative diseases such as: schizophrenia, Alzheimer's disease, Huntington's disease, Parkinson's disease, mitochondrial dysfunction and aging problems (e.g., [15–19]). There are evidences indicating that the activity of cytochrome oxidase, a key mitochondrial enzyme that catalyzes the reduction of oxygen to form water, is significantly impaired in schizophrenic [17] and Alzheimer's patients [18, 19]. Also the studies of diseases caused by mitochondrial DNA mutations suggests that a variety of neurodegenerative processes may be associated with defects in mitochondrial oxidative phosphorylation [20, 21]. Therefore, the cerebral metabolic rate of oxygen may provide an early biomarker of pathophysiology change in various brain disorders.

2.2 Concept of studying oxygen metabolism using ^{17}O NMR

The metabolic processes as illustrated in Fig. 1 can be assessed with various *in vivo* MR spectroscopy (MRS) techniques. For example, the glucose metabolism has been examined by *in vivo* ^{1}H and ^{13}C MRS [22, 23], and the ATP metabolism can be studied using *in vivo* ^{31}P MRS in combination with the magnetization transfer method [24–26]. In principle, *in vivo* ^{17}O MRS should be able to directly study the oxygen metabolism based on the following simple chemical reaction and the use of ^{17}O-isotope labeled oxygen gas ($^{17}O_2$):

$$4H^+ + 4e^- + {}^{17}O_2 \rightarrow 2H_2{}^{17}O. \quad [1]$$

Similar to what has been done with ^{15}O Positron Emission Tomography (PET) [27, 28], when oxygen gas enriched with the MR detectable ^{17}O isotope is introduced into the animal or human body, it binds to the hemoglobin in the blood through lung exchange, and then enters the brain via the arteries and blood circulation. The ^{17}O-labeled oxygen molecules will be metabolized in the brain mitochondrion to produce ^{17}O-labeled water ($H_2{}^{17}O$) molecules. The production rate of the metabolized $H_2{}^{17}O$ water reflects the rate of oxygen metabolism in the brain tissue. Thus, using the ^{17}O MRS or imaging technique to monitor the dynamic change of the $H_2{}^{17}O$ water content in the brain will provide important information regarding the oxygen metabolism of the brain tissue.

2.3 Early attempts of in vivo ^{17}O NMR studies

The simple concept of utilizing ^{17}O MR to study oxygen metabolism in living species had been recognized many years ago and attempted by several research labs around the world. In the late 1980s and early 1990s, ^{17}O-enriched $H_2{}^{17}O$ water was used as a potential T_2 (transverse relaxation time) contrast agent for the proton MRI by Hopkins' group and others for studying tissue perfusion in various animal models [29–33]. Meanwhile, Mateescu et al. demonstrated the *in vivo* ^{17}O MRS detection of nascent mitochondrial water in larva and mouse breathing air with ^{17}O-enriched oxygen gas [34, 35]; Aria et al. explored the feasibility of *in vivo* ^{17}O NMR for estimation of cerebral blood flow (CBF) and oxygen consumption in animal models of rat, rabbit and dog [6, 7, 36]; Pekar et al. reported that coarse $CMRO_2$ images (0.8cc nominal resolution) can be obtained in the cat brain using ^{17}O NMR imaging and ^{17}O-enriched oxygen gas [5, 37]; and Fiat et al. examined possible methods for determination of $CMRO_2$ and CBF in animal brain (and potentially in human brain) using *in vivo* ^{17}O MRS/MRI [38–40]. On the other hand, in the middle and late 1990s, Ronen et al. and Reddy et al. suggested that the ^{17}O-labeled $H_2{}^{17}O$ water could be detected by spin-echo proton imaging with ^{17}O decoupling [41–45] or proton $T_{1\rho}$ dispersion imaging [46, 47], respectively, and these indirect ^{1}H-(^{17}O) methods were used to image the $H_2{}^{17}O$ distribution in phantoms and animals.

Although these early efforts had demonstrated the important concept and feasibility of ^{17}O NMR for assessing brain oxygen metabolism, the technology advancement had been hampered substantially by the limitations in the sensitivity for detecting the metabolically generated $H_2{}^{17}O$ water, as well as the practical applicability for general *in vivo* studies of the oxygen metabolism in animal or human brain.

3. ^{17}O NMR for studying brain oxygen metabolism

In order to advance the ^{17}O NMR technology for studying brain oxygen metabolism, it is necessary to thoroughly understand the basic aspects of the ^{17}O NMR; for instance, the relaxivity and sensitivity of the ^{17}O signal as well as the factors that influence these properties. In addition, it is important to understand the pros and cons of the different

approaches for detecting the $H_2{}^{17}O$ signal and find an optimal method for imaging the dynamic changes of the $H_2{}^{17}O$ water *in vivo*. Furthermore, it is essential to develop a reliable method for quantifying the cerebral metabolic rate of oxygen based on ^{17}O MR measurements of the metabolized ^{17}O water signal. Finally, it is crucial to establish a simple and completely non-invasive $CMRO_2$ imaging approach for animal and human applications.

3.1. ^{17}O NMR properties in a biological system

^{17}O is a stable isotope of oxygen existing in nature. Unlike the common, abundant form of oxygen (^{16}O), ^{17}O is the only oxygen nuclei with a magnetic moment that can be detected by NMR. Different from the nuclei of ^{1}H, ^{31}P and ^{13}C used for most *in vivo* MR applications, ^{17}O has a spin quantum number of greater than ½ (I = 5/2) and possesses an electric quadrupolar moment. The ^{17}O nucleus in water can interact with the two protons, resulting in an ^{17}O signal being a 1:2:1 triplet at extremely low water concentration [48]. However, the ^{17}O triplets collapse to one single and well-defined $H_2{}^{17}O$ resonance peak in a biological sample due to rapid proton exchange and quadrupolar relaxation leading to a large effect of line broadening. This feature simplifies the ^{17}O MRS pattern for detecting the ^{17}O water signal in biological systems.

The ^{17}O natural abundance is only 0.037%, which is almost 30 times lower than that of ^{13}C and 2700 times lower than that of ^{1}H and ^{31}P. Moreover, the magnetogyric ratio (γ) of the ^{17}O, which is proportional to the Larmor frequency, is 7.4 times lower than that of ^{1}H. These facts result in the lowest NMR receptivity for ^{17}O spin compared to other spin nuclei commonly used for biomedical research and clinical studies. This low inherent NMR sensitivity has hindered the progress of ^{17}O NMR for *in vivo* MR studies especially at relatively low magnetic fields, despite its great potential for providing unique and vital biological information.

3.1.1. Relaxation properties of ^{17}O in tissue water—One critical aspect of ^{17}O NMR for *in vivo* applications is the ^{17}O relaxivity of water in biological samples. Relaxivity can affect the NMR detection sensitivity and ultimately determines the usefulness and applicability of *in vivo* ^{17}O NMR. The ^{17}O quadrupolar moment can interact with local electric field gradients and the temporal fluctuation in this interaction induced by molecular motion can dominate the ^{17}O relaxation processes and determine both the longitudinal relaxation time (T_1) and the transverse relaxation time (T_2) [49]. In the case of the water molecule, in which the extreme narrowing limit (*i.e.*, $\tau_c\omega \ll 1$, where τ_c is the rotational correlation time and ω is the ^{17}O Larmor frequency in radian units) is approximately applicable (except for the very small fraction of bound water), the values of ^{17}O T_1 and T_2 can be approximated by:

$$\frac{1}{T_2} \cong \frac{1}{T_1} = \frac{3\pi^2}{10}\left(\frac{2I+3}{I^2(2I-1)}\right)\left(1+\frac{\eta^2}{3}\right)\left(\frac{e^2Qq}{h}\right)^2\tau_c \quad [2]$$

where the term (e^2Qq/h) is the ^{17}O quadrupolar coupling constant for bulk water, and η is an asymmetry parameter ($0 \leq \eta \leq 1$) [49]. Thus, the ^{17}O T_1 and T_2 values can be estimated by:

$$\frac{1}{T_2} \cong \frac{1}{T_1} = 0.948\left(1+\frac{\eta^2}{3}\right)\left(\frac{e^2Qq}{h}\right)^2\tau_c. \quad [3]$$

Because the variables in Eq. [3] are independent upon the magnetic field strength (B_0), ^{17}O T_1, T_2 as well as apparent T_2 (T_2*) are expected to be insensitive to B_0. Taken the literature values of η=0.7, $e^2Qq/h = -8.1$ MHz and $\tau_c = 2.7\times10^{-12}$ s for bulk water at 25°C [50], the

estimated ^{17}O T_2 and T_1 according to Eq. [3] should be approximately 5.1 ms. This estimation indicates that the ^{17}O relaxation times of water are extremely short, in the range of few milliseconds.

The prediction of equal ^{17}O T_1 and T_2 values for the water molecules using Eq. [3] relies on the approximation of neglecting the effect of the ^{17}O-^{1}H scalar coupling. The actual ^{17}O water T_2 (or T_2*) value in a biological sample or water solution should be smaller than the ^{17}O T_1 value because of the combined effects of the ^{17}O-^{1}H scalar coupling and the proton exchange on the ^{17}O transverse relaxation process [51]. The proton exchange rate between $H_2{}^{17}O$ and $H_2{}^{16}O$ is sensitive to pH. At near-neutral pH, the scalar coupling has a maximal effect for enhancing the apparent ^{17}O transverse relaxation rate.

The ^{17}O longitudinal and transverse relaxation times of the natural abundance water in the rat brain have been explicitly measured and compared at field strengths of 4.7T versus 9.4T [52]. The relaxation times were found to be field independent (T_2=3.0 ms, T_2*=1.8 ms and T_1=4.5 ms at 4.7T versus T_2=3.0 ms, T_2*=1.8 ms and T_1=4.8 ms at 9.4T) [52]. These experimentally measured ^{17}O relaxation times are in line with the predicted values according to Eq. [3] and the reported values in the literature [38, 53]. Recent experimental evidence has indicated that the field-independence of the ^{17}O relaxivity can hold at much higher magnetic fields [54].

3.1.2. Pros and cons of extremely short ^{17}O-water relaxation times—The very short ^{17}O T_1 values of the brain $H_2{}^{17}O$ (several milliseconds) [38, 52] allow rapid NMR signal acquisitions at a given sampling time, thus, gaining signal-to-noise ratio (SNR) per unit time. The repetition time for acquiring the ^{17}O signal can be pushed to as short as tens of milliseconds. The major constraint is the potential concern of the specific absorption rate (SAR: a measure of the rate of absorption of RF energy in the body) allowed by FDA regulation.

The extremely short ^{17}O T_2* of the brain $H_2{}^{17}O$ (~2 ms) results in a broadening of the water resonance peak to a line width of 100–200 Hz *in vivo* and a substantial SNR reduction. It is crucial to minimize the delay (or echo time) between the ^{17}O spin excitation pulse and NMR signal sampling in order to avoid a substantial loss of the ^{17}O signal due to the rapid T_2* decay. The linewidth of the ^{17}O resonance peak of H_2O is relatively insensitive to the B_0 inhomogeneity (hence shimming quality) because of the intrinsically broad linewidth and the much lower ^{17}O magnetogyric ratio (7.4 times lower than that of ^{1}H). This fact implies that the requirement for B_0 homogeneity either in the bare magnet or together with room temperature shim compensation is considerably less stringent for *in vivo* ^{17}O NMR compared to *in vivo* ^{1}H, ^{31}P or ^{13}C NMR.

3.1.3. Advantage of ^{17}O NMR at high/ultrahigh magnetic field—One of the most important advantages provided by high/ultrahigh magnetic fields is the potential gain in NMR sensitivity. This is particularly crucial for *in vivo* ^{17}O NMR, where the inherent NMR sensitivity is extremely low. For a magnetic nucleus, the optimal SNR of the NMR signal acquired within a *unit time* at a given field strength depends on T_1, T_2*, B_0 and the RF coil quality factor (Q) according to [55–58]:

$$\text{SNR (per unit acqusition time)} \propto B_0^{\beta}\sqrt{\frac{QT_2^*}{T_1}}. \quad [4]$$

The parameter β was suggested to be approximately 7/4 based on theoretical predictions [56, 58]. Unlike the water proton spins in biological tissues, which are characterized by longer T_1

and shorter T_2 (or T_2*) with increased field strength, the field independence of ^{17}O relaxivity implies that the ^{17}O-water sensitivity gain at higher fields is not compromised by the relaxation times. Although the short T_2* (or broad linewidth) of the ^{17}O resonance peak in $H_2{}^{17}O$ leads to an effective reduction in the ^{17}O NMR sensitivity, this reduction can be partially compensated by the extremely short ^{17}O T_1 (< 5 ms in the brain), allowing rapid signal averaging [38, 52]. Therefore, it is possible to achieve a large sensitivity gain for *in vivo* ^{17}O NMR at high/ultrahigh fields.

The *in vivo* ^{17}O NMR sensitivity has been quantitatively compared at field strengths of 4.7T versus 9.4T [52]. The striking finding from this study, as shown in Fig. 2, is the consistent observation of approximately *four-fold* SNR gain at 9.4T compared to 4.7T indicating an approximated $7/4^{th}$ power dependence of ^{17}O SNR on B_0 as predicted by the NMR theory [52, 56, 58]. These results demonstrate the significant advantage provided by high field strength for the direct detection of ^{17}O NMR signal. The trend for increasing ^{17}O NMR sensitivity is likely to hold much beyond the field strength of 9.4T [54]. Compare to *in vivo* ^{1}H, ^{31}P or ^{13}C NMR, *in vivo* ^{17}O NMR is likely to benefit the most from the increasing field strength in terms of the NMR sensitivity gain.

3.1.4. In vivo NMR invisibility of $^{17}O_2$—In contrast to the ^{15}O-PET approach which is unable to distinguish the signals emitted by the ^{15}O atoms in the $^{15}O_2$ molecules from those in the metabolically generated $H_2{}^{15}O$ molecules; the ^{17}O resonance peak of the $^{17}O_2$ molecules, when bound to hemoglobin in the blood, is extremely broad because of very slow rotational motion of the large HbO_2 complex, and very difficult to detect with conventional *in vivo* ^{17}O NMR approaches. Saturation transfer electron paramagnetic resonance studies have shown that the τ_c value for the rotational motion of the hemoglobin molecule is $2{\cdot}10^{-8}$ s in solution and increases to $8{\cdot}10^{-6}$ s when the hemoglobin molecule is encapsulated within the erythrocyte [59]. This τ_c value is approximately 10^6 times slower than that of the free water. Such slow rotational motion leads to extremely fast ^{17}O T_2 relaxation according to Eq. [2] and renders the $^{17}O_2$ molecule bound to hemoglobin invisible for *in vivo* ^{17}O NMR detection.

The $^{17}O_2$ molecule while it is in the gas phase or dissolved in water is strongly paramagnetic due to its two unpaired electrons, and hence is undetectable in conventional NMR measurement because of the strong dipolar coupling between the electrons and the ^{17}O nucleus. Thus, the direct *in vivo* ^{17}O NMR approach will detect *only $H_2{}^{17}O$ but not $^{17}O_2$* in the biological sample.

This unique MR specificity for detecting ^{17}O-labeled water significantly simplifies the methodology for measuring and quantifying cerebral metabolic rate of oxygen ($CMRO_2$) because all ^{17}O-labeled components other than the metabolically generated $H_2{}^{17}O$ can be ignored, leading to a simple quantification scheme as illustrated in Fig. 3 [60].

3.2. Influence of ^{17}O-^{1}H scalar coupling on ^{1}H relaxation of water

The existence of an ^{17}O spin in the tissue water, either in natural abundance or at elevated enrichment levels, will affect the ^{1}H relaxation properties of the tissue. Half a century ago, Meiboom studied the proton chemical exchange in ^{17}O-enriched water solution at pH of neutral range [51]. It was found that the spin-spin coupling (i.e. scalar coupling) between the ^{1}H and the ^{17}O spins could shorten the proton transverse relaxation time or the rotating frame spin-lattice relaxation time ($T_{1\rho}$) but not the longitudinal relaxation time (T_1), and such scalar interaction of ^{17}O-^{1}H was modulated by the fast proton chemical exchange between the $H_2{}^{17}O$ and $H_2{}^{16}O$ molecules. Meiboom's finding provided a mechanism for indirect detection of the $H_2{}^{17}O$ signal using ^{1}H MR imaging. This indirect ^{1}H-(^{17}O) MR

approach was anticipated to better inherent NMR sensitivity than that of the direct ^{17}O MR approach [41].

3.2.1. Effect of ^{17}O-^{1}H scalar coupling on proton T_2 relaxation of tissue water

—The influence of the ^{17}O-^{1}H scalar coupling on the ^{1}H T_2 value ($T_{2,H}$) of the tissue water can be quantitatively described by [29, 41, 42, 51, 61]:

$$\frac{1}{T_{2,H}}=\frac{1}{T_{2,H}^{(16)}}+P\left(\frac{1}{T_{2,H}^{(17)}}-\frac{1}{T_{2,H}^{(16)}}\right)\approx\frac{1}{T_{2,H}^{(16)}}+\frac{35}{12}P\tau J^2, \quad [5]$$

where a ^{1}H chemical shift difference between $H_2{}^{17}O$ and $H_2{}^{16}O$ is neglected; $T_{2,H}^{(16)}$ and $T_{2,H}^{(17)}$ are the proton transverse relaxation times of $H_2{}^{17}O$ and $H_2{}^{16}O$, respectively; P is the molar fraction of $H_2{}^{17}O$ and is equivalent to the ^{17}O enrichment fraction; τ is the characteristic proton exchange lifetime in $H_2{}^{17}O$ and J is the ^{17}O-^{1}H scalar coupling constant. The relation described by Eq. [5] provides the basis for assessing the fractional content of $H_2{}^{17}O$ water (*i.e.*, P in Eq. [5]) through the change in proton T_2.

It was experimentally verified that the proton transverse relaxation rate indeed linearly correlates with the $H_2{}^{17}O$ concentration in biological solutions up to 5% enrichment, whereas the proton longitudinal relaxation time was not significantly affected by the ^{17}O enrichment [29]. Therefore, ^{17}O-labeled $H_2{}^{17}O$ can be used as an exogenous and/or endogenous contrast agent, respectively, for cerebral blood flow (CBF) and $CMRO_2$ measurements through measuring the change in the T_2-weighted ^{1}H MRI signal using a spin-echo sequence, for instance.

Several early studies observed proton signal reduction in the brain after the introduction of ^{17}O-labeled water [7, 29–32, 62], and its change can be linked to cerebral blood perfusion at different physiological conditions in normal and ischemic brain (*e.g.*, [31]). The time courses of the signal changes were successfully applied to quantify and image CBF for a wide range of CBF values induced by hypercapnia and hypocapnia in animals [7, 32]. Subsequently, this indirect ^{17}O detection approach was applied for imaging the signal change of the $H_2{}^{17}O$ metabolized from the ^{17}O-labeled oxygen gas [36, 63]. However, all these early studies were conducted in a qualitative manner and it was difficult to provide an absolute concentration of the ^{17}O-labeled water in the brain. Though this limitation should not be a problem for quantifying CBF in which only the relative concentration of $H_2{}^{17}O$ water in the brain is required, it does pose a hurdle for quantifying $CMRO_2$.

One improved method for quantifying the $H_2{}^{17}O$ tracer concentration is to introduce another proton spin-echo MRI in the presence of ^{17}O decoupling during the echo time (TE) and/or acquisition time [41–45]. The ^{17}O decoupling can abolish the interaction of the ^{1}H-^{17}O scalar coupling, and ultimately, suppress its effect on the water proton T_2 relaxation and increase the T_2 value. The difference of the proton spin-echo signals of $H_2{}^{17}O$ water in the presence and absence of ^{17}O decoupling provides a simple connection with the $H_2{}^{17}O$ content. The absolute $H_2{}^{17}O$ concentration can be calibrated by additional paired measurements of natural abundance $H_2{}^{17}O$ with a known concentration (*i.e.*, P = 0.037%) before introducing the $H_2{}^{17}O$ tracer. This indirect ^{17}O approach with ^{17}O decoupling was tested with phantom solutions and tissue models [41, 43–45]; it was also examined in the rat brain under normal physiological condition [42] and during focal cerebral ischemia [64] by injection of ^{17}O-labeled water tracer into the rat body. The results indicate that when an *adequate* amount of metabolic $H_2{}^{17}O$ is present in the brain, this indirect *in vivo* ^{17}O approach could potentially be used for quantifying and imaging $CMRO_2$.

3.2.2. Effect of ^{17}O-^{1}H scalar coupling on proton $T_{1\rho}$ relaxation of tissue water

—Another alternative indirect ^{17}O approach is to detect $H_2{}^{17}O$ by using the proton $T_{1\rho}$ dispersion imaging method [46, 47, 65]. This method applies single proton radiofrequency (RF) channel for acquiring $T_{1\rho}$-weighted proton images with two different spin locking RF powers. Although the mechanism underlying the $T_{1\rho}$ contrast in biological samples is not fully understood, the major contribution is likely to be from proton exchange [66], which can be potentially linked to the $H_2{}^{17}O$ concentration through ^{17}O-^{1}H scalar coupling and the chemical exchange between $H_2{}^{17}O$ and $H_2{}^{16}O$. Such an exchange, however, may not be the only process occurring in biological samples, and this complicates the $T_{1\rho}$ method and quantification for determining the $H_2{}^{17}O$ concentration. An example of this complication is the observation that $T_{1\rho}$ contrast changes in the animal brain during ischemia even without ^{17}O-labeled water tracer [67, 68]. Another complication is the difficulty of obtaining prior information on the intrinsic $T_{1\rho}$ dispersion of tissue, which is needed for absolute quantification. Nevertheless, this method has been successfully applied to determining CBF where the absolute $H_2{}^{17}O$ concentration is not required [69], and to imaging the CBF changes in tumors [70]. Recently, it has also been attempted for estimating the $CMRO_2$ in the animal brain [71–73].

3.2.3. Pros and cons of proton MRI for indirectly detecting ^{17}O-labeled metabolic water

—The major advantages of indirect ^{1}H-(^{17}O) approaches for detecting ^{17}O-labeled water in brain tissue is the high sensitivity of the proton signal and the ability to apply conventional MRI acquisition and data processing methods. In addition, the proton $T_{1\rho}$ dispersion imaging approach requires only a single proton RF channel and can be implemented on a clinical MRI scanner.

However, caution should be exercised when absolute quantification of the $H_2{}^{17}O$ concentration in a biological sample is required. Both ^{17}O-^{1}H scalar coupling and the chemical exchange between $H_2{}^{17}O$ and $H_2{}^{16}O$, the mechanisms responsible for the indirect ^{17}O detection, are all sensitive to many physiological parameters such as pH and temperature. This difficulty is evident from the experimental observations that equal concentrations of $H_2{}^{17}O$ tracer do not produce the same magnitude of T_2 change (or T_2-weigthed proton signal) in different physiological environments [29], and the detected change can completely disappear when pH is shifted away from neutral [64].

Furthermore, it should also be noted that although the intrinsic proton signal of the tissue water offered by indirect ^{1}H-(^{17}O) approach is much higher than the ^{17}O signal measured by the direct ^{17}O approach, the reproducibility or reliability of the ^{17}O-water signal detection in consecutively acquired datasets is far more crucial than the absolute signal (or SNR) acquired in a single dataset. This is because the ^{17}O-MR based $CMRO_2$ imaging approach relies on measuring the small dynamic changes of the metabolically generated $H_2{}^{17}O$ and their spatial distribution. In addition, the actual ^{1}H signal that is relevant to the tissue $H_2{}^{17}O$ content could be much smaller than the total available ^{1}H signal. For example, it has been shown that a 10% signal increase in the T_2-weighted ^{1}H MRI corresponded to about 0.45% of $H_2{}^{17}O$ content in the rat brain, which is over twelve times that of the natural abundance $H_2{}^{17}O$ level [42]. Therefore, the proton signal changes due to the metabolically generated $H_2{}^{17}O$ water in the T_2- or $T_{1\rho}$-weighted MR imaging, which is expected to be in the range of 1%, will likely be compromised by the signal fluctuation caused by the physiological noise (e.g., respiration or pulsation) or scanner instability [13].

Another potential technical limitation posed by both ^{17}O-decoupled and $T_{1\rho}$-based ^{1}H MRI approaches is the requirement of relatively large RF power either for ^{17}O decoupling or for the proton spin locking, in particular, for human applications at high magnetic fields.

3.3. Theory and quantification of $CMRO_2$ based on in vivo ^{17}O MRS/MRI approach

3.3.1. Theory and quantification model—As illustrated in Fig. 3, the dynamic change of the metabolically generated $H_2{}^{17}O$ concentration in the brain during an $^{17}O_2$ inhalation is affected by three parallel processes: (i) cerebral oxygen utilization for generating the metabolic $H_2{}^{17}O$ in the brain tissue; (ii) cerebral blood perfusion resulting in $H_2{}^{17}O$ washout from the brain, and (iii) blood recirculation bringing the metabolically generated $H_2{}^{17}O$ in the entire body back to the brain. All contributions from these three processes have to be considered for quantifying $CMRO_2$. Based on the Kety - Schmidt theory [74], the mass balance of the ^{17}O-isotope labeled $H_2{}^{17}O$ in the brain tissue during an $^{17}O_2$ gas inhalation can be derived as [5, 39, 60, 75]:

$$\frac{dC_b(t)}{dt}=2\alpha(t)f_1 CMRO_2+f_2 CBF(C_a(t)-C_v(t)), \quad [6]$$

where $C_a(t)$, $C_b(t)$ and $C_v(t)$ are the metabolic $H_2{}^{17}O$ concentrations in excess of the natural abundance $H_2{}^{17}O$ concentration in the arterial blood, brain tissue and venous blood; respectively, as a function of $^{17}O_2$ inhalation time (t, unit = minute); α(t) is the ^{17}O enrichment fraction of the oxygen atoms in the inhaled $^{17}O_2$ gas which could vary with inhalation time; and the factor of 2 accounts for the fact that two H_2O molecules are formed from one O_2 molecule through the oxidative metabolism according to Eq. [1]. Two unit conversion factors, $f_1=1.27$ and $f_2=1.05$, are used to achieve consistency of units among all parameters used in Eq. [6] [37, 60, 75].

The natural abundance $H_2{}^{17}O$ concentration can be used as an *internal reference* to calibrate the absolute values of $C_b(t)$, $C_a(t)$ and $C_v(t)$ with preferred units of *μmol/(g brain water)* for $C_b(t)$, *μmol/(g blood water)* for $C_a(t)$ and $C_v(t)$; and leads to the $CMRO_2$ unit of *μmole/min/(g* brain tissue).

Therefore, the $CMRO_2$ values can be precisely calculated by solving the linear differential Eq. [6] if the parameters of $C_b(t)$, α(t), CBF, $C_a(t)$ and $C_v(t)$ are known or can be measured.

3.3.2. $CMRO_2$ quantification for small animal models—The methods for quantifying $CMRO_2$ in the small animal case were first examined by Pekar and Fiat et al. [5, 37, 39, 40, 76]. The complete model of $CMRO_2$ quantification in the small animal was clearly demonstrated and established by Zhu et al. for fast imaging of $CMRO_2$ in rat brain within a few minutes of $^{17}O_2$ inhalation at high field [75]. In this comprehensive study, all parameters involving the oxygen metabolism and perfusion of the brain tissue as shown in Eq. [6] were experimentally determined via independent and concurrent ^{17}O MR measurements in the rat brain at 9.4T [75].

For a small animal such as a rat, due to its fast respiration and high heart rate, the labeled $^{17}O_2$ gas once introducing into the body, will quickly replace the regular $^{16}O_2$ gas to produce $H_2{}^{17}O$ water. Thus, the ^{17}O enrichment fraction can be approximated as a time independent constant, *i.e.* $\alpha(t) \approx \alpha$, and the transition time for $^{17}O_2$ to replace the $^{16}O_2$ gas is negligible compare to the total $^{17}O_2$ inhalation period (≥ few minutes). If one assumes that the water in the brain tissue is in equilibrium with water in the venous blood, then $f_2C_v(t) = C_b(t)/\lambda$ where λ is the brain/blood partition coefficient (≈ 0.90) with the unit of *(ml blood)/(g brain tissue)* [77]. Substituting this relation and introducing two new correction factors (*n* and *m*) into Eq. [6] leads to

$$\frac{dC_b(t)}{dt}=2\alpha f_1 CMRO_2+mCBF(f_2 Ca(t)-\frac{nC_b(t)}{\lambda}). \quad [7]$$

The correction factor *m* accounts for the water permeability restriction across the blood-brain burrier (BBB) [78]; and *n* accounts for the permeability restriction when the metabolically generated $H_2{}^{17}O$ molecules inside the mitochondria crosses the mitochondrial membranes [60, 75]. Both *m* and *n* depend on the CBF [60, 75]. The function of $C_a(t)$ (or artery input function) is determined by the total metabolic $H_2{}^{17}O$ generated in all aerobic organs of living body. It approximates as a linear function of $^{17}O_2$ inhalation time (i.e., $C_a(t) \approx At$, where *A* is a constant) [5, 6, 60, 75]. Thus, the solution for Eq. [7] becomes:

$$CMRO_2(t)=\frac{\left\{\left[\frac{C_b(t)-\frac{Af_2\lambda^2}{mn^2CBF}(\frac{mnCBF}{\lambda}te^{-\frac{mnCBF}{\lambda}t}+e^{-\frac{mnCBF}{\lambda}t}-1)}{1-e^{-\frac{mnCBF}{\lambda}t}}\right]-\frac{Af_2\lambda t}{n}\right\}}{\frac{2\alpha\lambda f_1}{mnCBF}}. \quad [8]$$

According to this equation, the $CMRO_2$ value at *each* data point measured at different inhalation time (*t*) can be precisely calculated using the experimentally measured CBF, *A* and *n* values, $C_b(t)$ time courses and other known constants (f_1, f_2, *m*, α and λ) [13, 60, 75].

Fig. 4 summaries the multiple *in vivo* ^{17}O MR measurements performed on anesthetized rat brains for imaging and quantifying $CMRO_2$ [13, 75]. The CBF measurement was performed via bolus injection of a small amount of ^{17}O-enriched $H_2{}^{17}O$ into one internal carotid artery and monitoring the washout process of the $H_2{}^{17}O$ tracer in the animal brain using 3D ^{17}O chemical shift imaging (CSI) [52]. Fig. 4A demonstrates the stacked plots of $H_2{}^{17}O$ spectra acquired from a single voxel of a 3D ^{17}O CSI data set in a representative rat before and after the $H_2{}^{17}O$ bolus injection. The peak height of the $H_2{}^{17}O$ spectra shows an exponential decay and its decay rate determines the CBF value in the CSI voxel [13, 52, 75]. The crucial step for $CMRO_2$ measurements is to monitor and image the dynamic changes of the metabolic $H_2{}^{17}O$ content in the brain (i.e., $C_b(t)$) during an inhalation of $^{17}O_2$ gas. Fig. 4B illustrates the stacked plots of ^{17}O spectra of cerebral $H_2{}^{17}O$ from one representative CSI voxel acquired before, during and after a 2-minute inhalation of $^{17}O_2$ [75]. It indicates excellent ^{17}O NMR sensitivity for detecting the cerebral $H_2{}^{17}O$ signal and its change during the inhalation; and the approximately linear increase of brain $H_2{}^{17}O$ during a short $^{17}O_2$ inhalation is evident, and the slope is tightly coupled to $CMRO_2$. The arterial input function $C_a(t)$ was measured *in vivo* by an implanted ^{17}O RF coil [79] wrapped around a carotid artery. Fig. 4C illustrates the implanted ^{17}O RF coil, the natural abundance $H_2{}^{17}O$ signal detected only from the rat carotid blood and the $C_a(t)$ time course measured during a two-minute inhalation of $^{17}O_2$ [75]. The experimental results show an approximately linear relation between the arterial $H_2{}^{17}O$ concentration and the $^{17}O_2$ inhalation time, and the linear regression of $C_a(t)$ gave the value of the constant *A* required by Eq. [7] and Eq. [8]. Finally, the ratio between the decay rates of $H_2{}^{17}O$ signal measured after the cessation of $^{17}O_2$ inhalation (see Fig. 4B) versus that after a $H_2{}^{17}O$ bolus injection (see Fig. 4A) gave the value of the constant *n* reflecting the $H_2{}^{17}O$ permeability restriction across the mitochondrial membranes [60, 75].

The CBF measurement can be performed concurrently with the $CMRO_2$ measurement on the same animal while $C_a(t)$ (see Fig. 4C) and $C_b(t)$ (see Fig. 4B) measurements can be conducted simultaneously with the configuration of dual ^{17}O RF coils and receivers [79]. The values of $C_b(t)$, CBF and *n* measured from each ^{17}O MRS imaging (MRSI) voxel and the value of *A* measured from each ^{17}O inhalation measurement in the same animal as

demonstrated in Fig. 4 can be used to calculate the absolute $CMRO_2$ value as a function of inhalation time according to Eq. [8]. Fig. 5A shows one example of $CMRO_2$ time course from a representative ^{17}O-CSI voxel with a temporal imaging resolution of 11 seconds [75]. It is evident that the $CMRO_2$ values are independent of the $^{17}O_2$ inhalation time if the first two $CMRO_2$ values characterized with relatively large fluctuations are excluded. These $CMRO_2$ values were averaged for improving measurement accuracy. The same procedure and calculation can be applied to all ^{17}O CSI voxels for generating 3D $CMRO_2$ images in the rat brain [12, 75]. Fig. 5B demonstrates three adjacent $CMRO_2$ images in the coronal orientation from a representative rat brain. The averaged $CMRO_2$ and CBF values in the rat brains anesthetized with α-chloralose were found to be 2.19±0.14 μmol/g/min and 0.53±0.07 ml/g/min (n=7), respectively [75]. These results are consistent with the literature reports using other independent techniques under similar physiological condition [80, 81].

3.3.3. $CMRO_2$ quantification in humans—Unlike small animals, quantification of $CMRO_2$ in humans faces serious challenges. The human body size, lung capacity and respiration rate as well as blood circulation speed are drastically different from those in the small animal. It is expected that the exchange process between non-labeled and inhaled ^{17}O-labeled oxygen gases in a human lung will be much slower compared to small animals such as a rat or mouse. Moreover, a much longer blood circulation time through the human body could further slow down the binding process of inhaled ^{17}O-labeled oxygen to the hemoglobin in the blood stream. Thus, the ^{17}O fractional enrichment of the oxygen gas in human artery blood (i.e., the α(t) term in Eq. [6]) will take much longer to reach a steady-state level (i.e., the ^{17}O enrichment α of the inhaled $^{17}O_2$ gas). For this reason, the $CMRO_2$ quantification model that worked well for the rat brain [75] failed to provide acceptable $CMRO_2$ values for a human study in which a short inhalation of $^{17}O_2$ gas (2–3 minutes) was employed [82].

Recently, Atkinson and Thulborn proposed a three-phase model for quantifying $CMRO_2$ in the human brain based on *in vivo* ^{17}O and ^{23}Na MR imaging data obtained at 9.4T [83]. In this model, the dynamic change of the $H_2{}^{17}O$ water in brain tissue was separated into three-phases: i.e., prior, during and after inhalation of $^{17}O_2$ gas; two rate constants K_L and K_G were utilized to represent the loss and gain of the $H_2{}^{17}O$ water within the imaging voxel, respectively; and a mass balance equation similar to Eq. [6] was used to describe the amount of the ^{17}O-labeled water in each voxel at each phase where the brain mass of the voxel was computed from co- registered ^{23}Na MRI data. The $CMRO_2$ as well as the rate constants K_L and K_G values for each imaging voxel were determined by performing a least-square fit of the dynamic $H_2{}^{17}O$ data for all three-phases. The key component of this model for applying to the $CMRO_2$ quantification in human is that it considered the transition of the ^{17}O fractional enrichment of the $^{17}O_2$ gas in arterial blood (i.e. the α(t) term of Eq. [6]). The transitions of α(t) from zero to α during the inhalation phase and from α to zero during washout phase after the inhalation were estimated based on the parameters of the pulmonary arteriovenous difference fraction ($F_{A\text{-}V}$) and the mean blood circulation time (T_C), in which their values were approximated from the literature reports [83].

Although there are still many uncertainties in the $CMRO_2$ quantification model for human application, especially for determining and validating the fractional enrichment of the $^{17}O_2$ gas α(t), the work of Atkinson and Thulborn does provide a forward step towards the quantitative study of the oxygen metabolism in human brain using the *in vivo* ^{17}O MR imaging approach at high/ultrahigh field.

3.4. Establishing a robust and noninvasive ^{17}O MR method for Imaging $CMRO_2$

3.4.1. Methods for imaging dynamic $H_2{}^{17}O$ water content of the brain tissue—

The most crucial measurement for determining the $CMRO_2$ value is to monitor the dynamic change of the $H_2{}^{17}O$ water content in brain tissue. Therefore, establishing a robust $CMRO_2$ imaging approach relies on the ability to reliably image the dynamic change of the $H_2{}^{17}O$ signals in the brain tissue with reasonable spatial and temporal resolution.

For the indirect ^1H-(^{17}O) detection approach, conventional T_2-weighted spin-echo or $T_{1\rho}$-weighted MR imaging technique can be used to acquire the proton signal change related to the variation in $H_2{}^{17}O$ water content (see detailed discussion in Section 3.2.). For direct ^{17}O-MR detection approach, however, the conventional MR imaging technique is no longer suitable for imaging the $H_2{}^{17}O$ signal because the T_2 (or T_2*) relaxation time of the $H_2{}^{17}O$ is extremely short, leading to severe signal loss or even disappearance if the echo time of the MR imaging sequence is relatively long compare to the transverse relaxation time of the ^{17}O-water (in the few millisecond range, see details in Section 3.1.).

So far, two MR imaging approaches with ultra-short echo time capability have been used for directly imaging the ^{17}O-water signal. One approach applies the flexible twisted projection [84] or a density-adapted 3D radial pulse sequence [85] commonly used for acquiring sodium MRI data; and the other approach images the $H_2{}^{17}O$ signals directly using the 3D chemical shift imaging (CSI) technique [86, 87]. Fig. 6 illustrates a typical 3D CSI sequence (Fig. 6A) used for the *in vivo* ^{17}O MR measurement and an example of the ^1H anatomic image as well as 3D ^{17}O-CSI data of the natural abundance $H_2{}^{17}O$ signal obtained from a representative rat brain (Fig. 6B). These *in vivo* ^{17}O-MR image data were acquired with approximately 0.1 ml of spatial resolution (nominal resolution: ~40μl) and total acquisition time of ~11 seconds at 9.4T. Regardless of which imaging sequence is chosen, the sensitivity and reliability of the ^{17}O-water signal obtained with the direct ^{17}O imaging approach depends in large extent on the echo time used for the imaging assuming comparable spatial and temporal resolutions are applied.

3.4.2. Feasibility of establishing a noninvasive $CMRO_2$ imaging approach—

As described earlier, the major technical limitation of the complete model for noninvasively determining $CMRO_2$ is the requirement of invasive measurements (e.g., CBF, $C_a(t)$, n). This will significantly limit the potential of this *in vivo* ^{17}O neuroimaging approach for broad biomedical applications, especially in humans. Thus, it is crucial to examine the feasibility of developing a completely noninvasive ^{17}O approach for imaging $CMRO_2$. Attempts have been made to simplify the experimental procedures and the models for determining $CMRO_2$ based on a number of approximations [5, 37, 39, 40, 60, 76].

One of these attempts, in which the invasive measurements could be eliminated completely by using the simplified model based on expanding $C_b(t)$ as a polynomial [60],

$$C_b(t)=a_1t+a_2t^2+a_3t^3+\cdots. \quad [9]$$

In this expansion, the first-order (or linear) coefficient of a_1 is directly proportional to $CMRO_2$ according to the following equation |[60]

$$|CMRO_2=\frac{a_1}{2\alpha f_1}, \quad [10]$$

where α and f_1 are known constants. Thus, using this *simplified model*, only the time course of $C_b(t)$ measured noninvasively by *in vivo* ^{17}O MR imaging is needed and it can be fitted to the polynomial function in Eq. [9] to calculate the linear coefficient of a_1, and ultimately determining $CMRO_2$ according to Eq. [10]. For practical applications with adequate SNR, a quadratic polynomial function usually provides a good approximation for fitting the time course of $C_b(t)$ with a moderated fitting error |[60]. It has been demonstrated that the $CMRO_2$ value obtained based on the complete model with invasive procedures has no statistical difference from that based on the simplified model and quadratic function fitting where only a single noninvasive measurement of $C_b(t)$ is required |[60]. Moreover, the results also indicate that the linear fitting of $C_b(t)$ could provide a good approximation for determining $CMRO_2$ in the rat brain when the $^{17}O_2$ inhalation time is relatively short (e.g., 2 minutes) |[60]. In another study, the simplified model was examined for determining $CMRO_2$ under varied physiological conditions |[88]; and the $CMRO_2$ results obtained with the complete model were compared with the simplified model using linear fitting of $C_b(t)$ under normothermia (37°C) and hypothermia (32°C) condition, which is a well known factor leading to significant suppression of both CBF and $CMOR_2$. Fig. 7 demonstrates an excellent consistency of the $CMRO_2$ results between the complete and simplified models for either the voxel-based comparison (Fig. 7A) or the averaged $CMRO_2$ comparison (Fig. 7B) at both brain temperatures |[88]. The comparison results reveal the validity of the simplified ^{17}O approach for imaging $CMRO_2$ applicable for small animal work across a wide physiological range

The ability to non-invasively image $CMRO_2$ in human brain is even more crucial. However, the above mentioned simplified method by linear or quadratic fitting of the $C_b(t)$ data is no longer appropriate because of the time dependent ^{17}O fractional enrichment of the $^{17}O_2$ gas (see details in Section 3..3.3) in humans. The quantification method based on the three-phase model has the potential for non-invasively mapping $CMRO_2$ in humans after careful validation and improvement |[83]. It is anticipated that additional technical developments which further advance the *in vivo* ^{17}O methodology could ultimately provide the simplest and completely non-invasive ^{17}O neuroimaging approach for imaging $CMRO_2$ in both animal and human brains.

3.4.3. Reliability and reproducibility of the $CMRO_2$ measurement—Another merit of the ^{17}O $CMRO_2$ imaging approach is its ability for performing repeated $CMRO_2$ imaging measurements with a short interval between two measurements. This is because the cerebral $H_2{}^{17}O$ concentration can quickly reach a new and steady level after the cessation of a brief $^{17}O_2$ inhalation, which allows repeated $CMRO_2$ measurements in the same subject and experimental session (see Fig. 8A for an example). Fig. 8B shows the excellent reproducibility of repeated $CMRO_2$ measurements in five rats (1^{st} measured $CMRO_2$ = 2.26 ± 0.18; 2^{nd} measured $CMRO_2$ = 2.20 ± 0.14 μmol/g/min; $CMRO_2$ ratio between the 1^{st} and 2^{nd} measurements = 1.03 ± 0.05; n=5) where $CMRO_2$ values were determined solely from the dynamic change of the ^{17}O-water signals |[88]. The results demonstrate the robustness and reliability of the simplified *in vivo* ^{17}O NMR approach for noninvasively and rapidly imaging $CMRO_2$ repeatedly in the small brain of a rat. This capability is particularly valuable for studies aiming at $CMRO_2$ changes induced by physiological or pathological perturbations in which multiple measurements are required under different conditions (e.g., control versus stimulation for brain function study). Therefore, it is likely that, at least in small animal brains, the combination of the simplified model and ultrahigh-field *in vivo* ^{17}O MRS may provide an alternative neuroimaging modality for studying the central role of oxidative metabolism in brain function and neurological diseases |[12, 13].

3.4.4. Detectability of the $CMRO_2$ change—The detectability of the changes in $CMRO_2$ is another important aspect of the high-field ^{17}O-MR based $CMRO_2$ imaging

approach that requires careful evaluation for *in vivo* applications. It is well documented that the basal $CMRO_2$ is sensitive to the brain temperature (see te>|[89, 90] and the references cited therein). Most studies reported in the literature, however, were based on the global $CMRO_2$ measurements of entire brain using the Kety-Schmidt method te>|[74, 91] and were lacking spatial information regarding the regional oxygen consumption rate and/or its change. A $CMRO_2$ imaging study using a 3D *in vivo* ^{17}O-CSI approach was designed and conducted at 9.4T for quantifying absolute $CMRO_2$ values in the rat brain at normal brain temperature (37°C) (i.e., normothermia) and mild hypothermia (32°C) conditions te>|[88]. Fig. 9A illustrates an example showing three representative slices of 3D $CMRO_2$ images from a rat brain under normothermic and hypothermic conditions. These images clearly show significant reduction of $CMRO_2$ crossing the entire brain induced by lowering brain temperature by several degrees. This metabolic suppression occurring at hypothermia was consistently observed in all five rats studied (Fig. 9B), resulting in an average of 45% $CMRO_2$ reduction as compared to normothermic condition te>|[88]. These findings indicate that the established *in vivo* ^{17}O MR imaging approach is sufficiently sensitive for determining the dynamic $CMRO_2$ change and its spatial distribution resulting from physiological perturbations. Thus, the measured $CMRO_2$ values can be quantitatively correlated with other associated physiological parameter(s). Fig. 10 illustrates one example showing the quantitative relation between $CMRO_2$ and CBF: both of these were measured by the direct *in vivo* ^{17}O MR approach in the α-chloralose anesthetized rat under a wide range of physiological conditions from normothermia to hypothermia te>|[88].. It clearly shows a strong correlation between CBF and $CMRO_2$ with a linear correlation coefficient of R = 0.97 indicating a tight vascular-metabolic coupling in the rat brain.

4. Current status of high-field *in vivo* ^{17}O MRS/MRI for studying brain bioenergetics

Since early 2000, substantial efforts have been devoted to the development of the high-field ^{17}O MRS/MRI approach for noninvasively imaging $CMRO_2$ with a short $^{17}O_2$ inhalation, which were mainly carried out using small animal models te>|[12, 54, 60, 75, 79, 88, 92, 93].. These research works have demonstrated not only the feasibility but also the great promise of the high-field ^{17}O MR approach for studying the central roles of oxidative metabolism in a living brain under various physiological conditions. Here, we highlight the major advance made in this regard, which represent the current status of the ^{17}O MR technology for $CMRO_2$ imaging.

4.1. Direct imaging of $CMRO_2$ in animal models

For directly imaging $CMRO_2$ in animal models, several major steps were taken to ensure the quality and reliability of the $CMRO_2$ measurement. Specifically, the development of the high-field in vivo ^{17}O-MR based $CMRO_2$ imaging approach has gone through the following processes: *1) feasibility assessment*, where relaxation properties and detection sensitivity of the natural abundance ^{17}O-water of brain tissue were examined at different magnetic field strengths te>|[52, 54, 92].; *2) methodology development*, where a comprehensive and quantitative *in vivo* 3D ^{17}O-CSI approach was established to image $CMRO_2$ in rat brains at 9.4T with only two minutes of $^{17}O_2$ inhalation te>|[79, 94].; *3) quantification and validation*, where a complete $CMRO_2$ quantification model as well as a simplified non-invasive $CMRO_2$ imaging method were established and validated for improving reliability and reproducibility te>|[60, 75, 88]., and *4) applicability assessment*, where the ability of the high-field ^{17}O MR approach for imaging $CMRO_2$ and its change in animal brains under various physiological conditions were demonstrated te>|[75, 88, 93].. Accordingly, the *in vivo* ^{17}O MRS/MRI approach, with a brief introduction of the $^{17}O_2$ gas, can be readily

applied to image the absolute $CMRO_2$ in small animal models at high/ultra-high fields for various physiological, neurological or pathological studies.

4.2. $CMRO_2$ image of the human brain

The ultimate goal for developing the $CMRO_2$ imaging approach is to study the oxygen metabolism in healthy and diseased human brains. Several attempts have been made to image $CMRO_2$ in the human brain te>|[38, 82, 83, 95, 96].. Fiat and coworkers examined the natural abundance ^{17}O-water signal of the human brain using 1.5T whole body clinical scanner. However, the extremely short relaxation times ($T_1 \leq 5$ms and $T_2 \approx 2$ms) and the poor sensitivity of the ^{17}O-MR signal available at 1.5T led to very low spatial and/or temporal resolution of the ^{17}O-MR imaging te>|[38, 95].. Zhu and coworkers have investigated the relaxivity and sensitivity of natural abundance ^{17}O-water in the human occipital lobe utilizing a 7T scanner te>|[82].. The results confirmed the advantage of the high magnetic field, which had been observed in animal models, for substantially improving the ^{17}O detection sensitivity, and which makes it possible to image the dynamic change of the $H_2{}^{17}O$ signal in human brain during a 2-min $^{17}O_2$ inhalation with excellent temporal resolution (11 sec) and reasonable spatial resolution (<1.4 cc nominal resolution). Fig. 11 displays the time courses of the $H_2{}^{17}O$ signals in two 3D-CSI voxels obtained from an representative subject before, during and after a brief $^{17}O_2$ gas inhalation (only 2 min), and it clearly demonstrates the feasibility of the ^{17}O MR approach for imaging the human brain $CMRO_2$ at the high field of 7T te>|[82]. Recently, Atkinson and Thulborn applied direct ^{17}O MR detection and ultra-short echo imaging sequence by using a 9.4T scanner for mapping $CMRO_2$ of entire human brain te>|[83].. The spatial (~2.7cc) and temporal (42 sec) resolutions of the 3D ^{17}O image achieved in this study were utilized for mapping the dynamic change of the ^{17}O water contents before, during and after ~15min $^{17}O_2$ gas inhalation in one human subject. With a three-phase $CMRO_2$ quantification model and co-registered ^{23}Na images for anatomic reference and brain tissue mass computation, 3D $CMRO_2$ maps of the entire human brain were obtained te>|[83] at 9.4T. The $CMRO_2$ values determined in this MR study were in a similar range to those reported from PET studies te>|[27]

Despite these advances, quantitative and noninvasive mapping of $CMRO_2$ in human brain still face many technical and methodological challenges (see more discussion in Section 5). Further research efforts are needed before the ^{17}O-MR based approach can be readily applied for studying oxygen metabolism in human brains.

4.3. Mapping functional $CMRO_2$ changes

One important application of the $CMRO_2$ imaging technique is to determine the $CMRO_2$ changes due to the functional activation of the brain. The BOLD (blood-oxygen-level dependence) contrast based functional MR imaging (fMRI) technique is the most widely used neuroimaging modality for studying brain function and human behavior te>|[97–100].. However, the BOLD-fMRI is unable to directly detect neuronal activity; instead, it relies on a complex interplay among CBF, cerebral blood volume (CBV), and $CMRO_2$ changes induced by altered brain activity te>|[101].. Precise interpretation of fMRI results requires a better understanding of the quantitative relationship between the fMRI BOLD contrast and the underlying neurophysiology—in particular the stimulus-evoked $CMRO_2$ change te>|[102]..

The ability to map the functional $CMRO_2$ changes induced by an external brain stimulus has recently been explored in a lightly anesthetized cat brain. Absolute $CMRO_2$ images with reasonable spatial and temporal resolutions were obtained from each cat during both resting and activation (visual stimulation) states, respectively te>|[93] and functional maps of the

relative $CMRO_2$ changes (i.e. $\Delta CMRO_2/CMRO_2$) were generated accordingly for each animal. Fig. 12 summarizes the findings of this study. In addition to observing significant $CMRO_2$ increases during the visual stimulation, the size and location of the activated brain regions depicted in the functional $\Delta CMRO_2/CMRO_2$ maps largely coincide with those regions showing positive BOLD-fMRI changes in the same cat brain despite the different spatial resolutions of the $CMRO_2$- and BOLD-based functional images (Fig. 12A). In addition, by directly imaging the absolute $CMRO_2$ values under both resting and activated brain states (Fig. 12B), this functional ^{17}O-$CMRO_2$ study not only provided a quantitative measure of relative $CMRO_2$ change elevated by visual stimulation (Fig. 12C) but also revealed a strong influence of baseline metabolic activity level on the relative $CMRO_2$ change in response to brain stimulation (Fig. 12D). Thus, this crucial finding regarding the quantitative relationship between the absolute $CMRO_2$ change and increased brain activity during activation suggests a tight neural-metabolic coupling and the vital role of oxygen metabolism in supporting the intensified neuronal activity in a working brain te>|[93]..

4.4. Ultra-fast $CMRO_2$ measurements

The ^{17}O-MR sensitivity achievable at high magnetic field can be used to image $CMRO_2$ with a much improved temporal resolution while sacrificing the spatial resolution to a certain extent. An ultra-fast $CMRO_2$ measurement strategy has been tested in the rat model at 9.4T. Fig. 13 demonstrates an example of the dynamics of the $H_2{}^{17}O$ contents before, during and after a 2 min $^{17}O_2$ inhalation in a rat brain from measurements acquired with high temporal resolution of *1 s* (see Fig. 13A); the averaged $CMRO_2$ value during the inhalation period in this case was found to be 1.32 μmol/g/min using the complete quantification model described in Eq. [8] (see Fig. 13B) and 1.43 μmol/g/min (linear fit) or 1.34 μmol/g/min (quadratic fit) using the simplified model described in Eqs. [9] and [10]. The simplified quantification model provides a reasonable approximation and, most importantly, it allows completely non-invasive determination of the absolute $CMRO_2$ value *in vivo*.

The ultra-fast temporal resolution of the $CMRO_2$ measurement enables the study aiming at rapid temporal changes in the oxygen consumption rate caused by instantaneous physiological or pathological alteration occurs in the animals. Two examples of such a study are shown in Fig. 14. The significant slow down or diminishing of the oxygen metabolism in the rat brain due to global ischemia (Fig. 14A) or heart arrest (Fig. 14B) is reflected in the sudden decrease or halt in the production of the ^{17}O-labeled metabolic water te>|[103].. Thus, through careful experimental design as shown in Fig. 14, the $CMRO_2$ values for the two different conditions (i.e., before and after ischemia or KCl injection) can be determined with only one short $^{17}O_2$ inhalation of a few minutes te>|[103]..

4.5. Simultaneous $CMRO_2$ and CBF imaging

As described earlier, the *in vivo* ^{17}O MR imaging approach at high/ultrahigh field has been established for non-invasively mapping $CMRO_2$ in small animals. However, imaging of CBF using the same ^{17}O MR approach usually requires invasive procedures for introducing the NMR-visible $H_2{}^{17}O$ as exogenous tracer. Experimental evidence reveals that the metabolic $H_2{}^{17}O$ water generated from a brief $^{17}O_2$ gas inhalation in the brain tissue had a much slower washout (or decay) rate compared to that of bolus $H_2{}^{17}O$ tracer, suggesting possible water permeability restrictions in the mitochondrial and/or cellular membranes te>|[75].. Nevertheless, further investigation found that the decay rate of the metabolic $H_2{}^{17}O$ after cessation of the $^{17}O_2$ gas inhalation was still closely related to the cerebral perfusion and its change; and a linear relationship between CBF and $H_2{}^{17}O$ decay rate was determined experimentally from combined CBF and $CMRO_2$ measurements in the rat brains under varied physiological or pathological conditions te>|[104]..

Fig. 15 shows an example of such multiple $CMRO_2$ and CBF measurements where the relative CBF values were also assessed using Laser Doppler Flowmeter (LDF) performed in a representative rat brain after undergoing global forebrain ischemia preparation. The metabolic $H_2{}^{17}O$ decay rates obtained in the $CMRO_2$ measurements during baseline, reperfusion and post-ischemia periods are displayed (see Fig. 15A) and their changes correlate well with the relative CBF changes measured by LDF (see Fig. 15B). The linear regression of the experimental data from similar measurements in different animals with different preparations for altering the brain perfusion led to the relation of CBF ≈ 1.86 × *k* (correlation coefficient R = 0.85), indicating that the measured metabolic ^{17}O-water decay rate *k* provides a good approximation for estimating CBF in a wide range of physiological (or pathological) conditions te>|[104]..

The findings from these researches demonstrate that *in vivo* ^{17}O MRS/MRI approach is capable of assessing not only $CMRO_2$ but also CBF simultaneously and noninvasively in the rat brain, and thus it provides a new utility for imaging the oxygen extraction fraction (OEF) of the brain tissue, another important physiological parameter, which is proportional to the ratio of $CMRO_2$ and CBF.

5. Challenge and Perspective

As described in this article, the most interesting and important application of *in vivo* ^{17}O NMR is for quantitatively imaging the rate of cerebral oxygen consumption occurring in mitochondria. Questions related to this rate are encountered frequently in biomedical research when considering either normal brain function or abnormalities related to a variety of brain diseases. Relevant to normal brain function, a question of whether the alterations in $CMRO_2$, cerebral metabolic rate of glucose (CMR_{glc}) and CBF induced by neuronal activity are quantitatively coupled (or matched) is central for understanding the mechanisms underlying most modern neuroimaging techniques including fMRI and PET. On the other hand, the central role of oxidative metabolism and its metabolic rate is also evident in pathologies associated with many brain disorders. Therefore, the ability to quantitatively *image* $CMRO_2$ *in vivo* is essential for efforts aimed at investigating and understanding cerebral oxidative metabolism under normal and pathological conditions. The promising *in vivo* ^{17}O NMR results as demonstrated during the past two decades and reviewed here have provided a crucial step towards the ultimate goal of developing a robust and completely noninvasive ^{17}O NMR approach for imaging $CMRO_2$ in animal brains, and potentially in human brains.

The establishment of high-field *in vivo* ^{17}O NMR for imaging $CMRO_2$ in small animal brains is quite successful while application of this method to the human brain faces some serious challenges. Firstly, the NMR sensitivity per unit tissue volume is reduced for human applications because the enlarged RF coil size (*i.e.*, reduced reception sensitivity) needed for covering the entire human brain, which is approximately 700 times larger than the rat brain. This disadvantage can be partially compensated for by increasing the ^{17}O imaging voxel size in quantification in humans and using advanced RF array coil technology. Secondly, the $CMRO_2$ human brain is more difficult due to the uncertainty in determining the kinetics of the ^{17}O fractional enrichment of the $^{17}O_2$ gas and other parameters. The last but not least challenge for routine $CMRO_2$ imaging, especially for human study, is the cost of $^{17}O_2$ gas. Currently, the cost of the ^{17}O-labeled oxygen gas is high because of the extremely low ^{17}O natural abundance, low production efficiency for achieving high ^{17}O enrichment, and presumably the low demand. Only a few companies are capable of supplying a large amount of $^{17}O_2$ now. However, it is reasonable to expect that further progress in the technical developments of *in vivo* ^{17}O approaches should stimulate numerous biomedical applications including clinical diagnosis, and increase the demand, ultimately leading to more

efficient $^{17}O_2$ production and lower retail prices. In addition to reduce the cost of the ^{17}O-$CMRO_2$ measurement, it is also essential to improve the efficiency of the $^{17}O_2$ gas delivery system and to minimize the lost or waste of the ^{17}O-labeled oxygen gas in the process.

In conclusion, the high/ultrahigh field NMR systems currently available or in development for both animals and humans provide great opportunities for *in vivo* MRI/MRS applications in medicine, especially for those nuclei with a low magnetogyric ratio. One of the nuclei that benefit the most from ultrahigh field strength is the ^{17}O spin combined with direct *in vivo* ^{17}O NMR detection, which has shown great promise for imaging $CMRO_2$ noninvasively. Finally, the successful developments of *in vivo* ^{17}O NMR approaches will lead to an alternative or better $CMRO_2$ neuroimaging tool compared to the established PET method, and could have a profound impact on the study of oxidative metabolism in brains and potentially in other organs such as hearts te>|[84, 105].

Acknowledgments

We are grateful for the technical assistance, support and participation from Drs. Nanyin Zhang, Xiaoliang Zhang, Hao Lei, Yi Zhang, Run-Xia Tian, Hellmut Merkle, Jae-Hwan Kwag, Pete Thelwall, Peter Andersen, Gregor Adriany and Kamil Ugurbil, and Mr. John Strupp and Hannes Wiesner. We also like to acknowledge Drs. Gheorghe D. Mateescu, Xin Yu, Chris Flask, Gil Navon, Itamar Ronen, Robert G. Shulman, Fahmeed Hyder, Seiji Ogawa, Joseph J.H. Ackerman, Alan C. McLaughlin, Keith Thulborn, Jie Zheng and Steve Blackband for scientific discussion and stimulation.

The work as reviewed in this article was supported partly by NIH grants of NS41262, EB02632, NS39043, EB00329, EB00513, NS057560, NS070839, P41 RR08079 and P30NS057091; and the Keck Foundation.

Abbreviations

γ	magnetogyric ratio
T_1	longitudinal relaxation time
T_2	transverse relaxation time
T_2*	apparent T_2
τ_c	rotational correlation time
B_0	magnetic field strength
SNR	signal-to-noise ratio
Q	RF coil quality factor
CSI	chemical shift imaging
ATP	adenosine triphosphate
ADP	adenosine diphosphate
Pi	inorganic phosphate
CBF	cerebral blood flow
LDF	laser Doppler flowmeter
BBB	brain-blood-barrier
CMR_{glc}	cerebral metabolic rate of glucose utilization
α	^{17}O enrichment fraction of inhaled
$CMRO_2$	cerebral metabolic rate of oxygen utilization

PET	positron emission tomography
fMRI	functional magnetic resonance imaging
$\mathbf{C_a(t)}$	time-dependent $H_2{}^{17}O$ concentration in excess of the natural abundance $H_2{}^{17}O$ concentration level in the arterial blood
$\mathbf{C_b(t)}$	time-dependent $H_2{}^{17}O$ concentration in excess of the natural abundance $H_2{}^{17}O$ concentration level in the brain tissue
$\mathbf{C_v(t)}$	time-dependent $H_2{}^{17}O$ concentration in excess of the natural abundance $H_2{}^{17}O$ concentration level in the venous blood
λ	brain/blood partition coefficient $^{17}O_2$ gas

References

1. Alder F, Yu FC. On the Spin and Magnetic Moment of ^{17}O. Phys Rev. 1951; 81:1067–1068.
2. Gerothanassis IP. Oxygen-17 NMR spectroscopy: Basic principles and applications (Part I). Progr NMR Spectr. 2010; 56:95–197.
3. Gerothanassis IP. Oxygen-17 NMR spectroscopy: Basic principles and applications (Part II). Progr NMR Spectr. 2010; 57:1–110.
4. Mateescu GD, Yvars GM, LaManna JC, Lust WD, Sudilovsky D. Oxygen-17 MRS: In vivo evaluation of water uptake and residence time in the mouse brain after injection of O-17 labeled water. Proc Inter Soc Magn Reson Med. 1990:1236.
5. Pekar J, Ligeti L, Ruttner Z, Lyon RC, Sinnwell TM, van Gelderen P, Fiat D, Moonen CT, McLaughlin AC. In vivo measurement of cerebral oxygen consumption and blood flow using ^{17}O magnetic resonance imaging. Magn Reson Med. 1991; 21:313–319. [PubMed: 1745131]
6. Arai T, Mori K, Nakao S, Watanabe K, Kito K, Aoki M, Mori H, Morikawa S, Inubushi T. In vivo oxygen-17 nuclear magnetic resonance for the estimation of cerebral blood flow and oxygen consumption. Biochem Biophys Res Commun. 1991; 179:954–961. [PubMed: 1898415]
7. Arai T, Nakao S, Morikawa S, Inubushi T, Yokoi T, Shimizu K, Mori K. Measurement of local cerebral blood flow by magnetic resonance imaging: in vivo autoradiographic strategy using ^{17}O-labeled water. Brain Res Bull. 1998; 45:451–456. [PubMed: 9570714]
8. Mateescu GD, Yvars GM, Dular T. Oxygen-17 Magnetic Resonance Imaging. Proc Inter Soc Magn Reson Med. 1987:929.
9. Mateescu GD, Fercu D. Interleave $^{17}O/\ ^{31}P$ MRS: Novel Approach for *In Vivo* Determination of Defects in Oxidative Phosphorylation. Proc Inter Soc Magn Reson Med. 1993:110.
10. de Graaf RA, Brown PB, Rothman DL, Behar KL. Natural abundance ^{17}O NMR spectroscopy of rat brain in vivo. J Magn Reson. 2008; 193:63–67. [PubMed: 18456525]
11. Mateescu GD. Functional oxygen-17 magnetic resonance imaging and localized spectroscopy. Adv Exp Med Biol. 2003; 510:213–218. [PubMed: 12580430]
12. Chen, W.; Zhu, XH.; Ugurbil, K. Imaging Cerebral Metabolic Rate of Oxygen Consumption ($CMRO_2$) using ^{17}O NMR Approach at Ultra-high Field. In: Shulman, RG.; Rothman, DL., editors. Brain Energetics and Neuronal Activity. John Wiley & Sons Ltd; New York: 2004. p. 125-146.
13. Zhu XH, Zhang N, Zhang Y, Zhang X, Ugurbil K, Chen W. In vivo ^{17}O NMR approaches for brain study at high field. NMR Biomed. 2005; 18:83–103. [PubMed: 15770611]
14. Rolfe DF, Brown GC. Cellular energy utilization and molecular origin of standard metabolic rate in mammals. Physiol Rev. 1997; 77:731–758. [PubMed: 9234964]
15. Beal MF. Does impairment of energy metabolism result in excitotoxic neuronal death in neurodegenerative illnesses? Ann Neurol. 1992; 31:119–130. [PubMed: 1349466]
16. Frackowiak RS, Herold S, Petty RK, Morgan-Hughes JA. The cerebral metabolism of glucose and oxygen measured with positron tomography in patients with mitochondrial diseases. Brain. 1988; 111:1009–1024. [PubMed: 3263167]

17. Maurer I, Zierz S, Moller H. Evidence for a mitochondrial oxidative phosphorylation defect in brains from patients with schizophrenia. Schizophr Res. 2001; 48:125–136. [PubMed: 11278159]
18. Maurer I, Zierz S, Moller HJ. A selective defect of cytochrome c oxidase is present in brain of Alzheimer disease patients. Neurobiol Aging. 2000; 21:455–462. [PubMed: 10858595]
19. Wong-Riley M, Antuono P, Ho KC, Egan R, Hevner R, Liebl W, Huang Z, Rachel R, Jones J. Cytochrome oxidase in Alzheimer's disease: biochemical and histochemical, and immunohistochemical analyses of the visual and other systems. Vision Res. 1997; 37:3593–3608. [PubMed: 9425533]
20. Wallace DC. Mitochondrial genetics: a paradigm for aging and degenerative diseases? Science. 1992; 256:628–632. [PubMed: 1533953]
21. Wallace DC. Mitochondrial diseases in man and mouse. Science. 1999; 283:1482–1488. [PubMed: 10066162]
22. Chen W, Novotny EJ, Zhu XH, Rothman DL, Shulman RG. Localized ^{1}H NMR measurement of glucose consumption in the human brain during visual stimulation. Proc Natl Acad Sci USA. 1993; 90:9896–9900. [PubMed: 8234332]
23. Gruetter R, Novotny EJ, Boulware SD, Rothman DL, Mason GF, Shulman GI, Shulman RG, Tamborlane WV. Direct measurement of brain glucose concentrations in humans by ^{13}C NMR spectroscopy. Proc Natl Acad Sci USA. 1992; 89:1109–1112. [PubMed: 1736294]
24. Du F, Zhu XH, Zhang Y, Friedman M, Zhang N, Ugurbil K, Chen W. Tightly coupled brain activity and cerebral ATP metabolic rate. Proc Natl Acad Sci USA. 2008; 105:6409–6414. [PubMed: 18443293]
25. Lei H, Ugurbil K, Chen W. Measurement of unidirectional Pi to ATP flux in human visual cortex at 7 T by using in vivo ^{31}P magnetic resonance spectroscopy. Proc Natl Acad Sci USA. 2003; 100:14409–14414. [PubMed: 14612566]
26. Shoubridge EA, Briggs RW, Radda GK. ^{31}P NMR saturation transfer measurements of the steady state rates of creatine kinase and ATP synthetase in the rat brain. FEBS Letters. 1982; 140:289–292. [PubMed: 6282642]
27. Mintun MA, Raichle ME, Martin WR, Herscovitch P. Brain oxygen utilization measured with O-15 radiotracers and positron emission tomography. J Nucl Med. 1984; 25:177–187. [PubMed: 6610032]
28. Ter-Pogossian MM, Eichling JO, Davis DO, Welch MJ. The measure in vivo of regional cerebral oxygen utilization by means of oxyhemoglobin labeled with radioactive oxygen-15. J Clin Invest. 1970; 49:381–391. [PubMed: 5411789]
29. Hopkins AL, Barr RG. Oxygen-17 compounds as potential NMR T_2 contrast agents: enrichment effects of $H_2{}^{17}O$ on protein solutions and living tissues. Magn Reson Med. 1987; 4:399–403. [PubMed: 3586987]
30. Hopkins AL, Haacke EM, Tkach J, Barr RG, Bratton CB. Improved sensitivity of proton MR to oxygen-17 as a contrast agent using fast imaging: detection in brain. Magn Reson Med. 1988; 7:222–229. [PubMed: 3398769]
31. Hopkins AL, Lust WD, Haacke EM, Wielopolski P, Barr RG, Bratton CB. The stability of proton T_2 effects of oxygen-17 water in experimental cerebral ischemia. Magn Reson Med. 1991; 22:167–174. [PubMed: 1798391]
32. Kwong KK, Hopkins AL, Belliveau JW, Chesler DA, Porkka LM, McKinstry RC, Finelli DA, Hunter GJ, Moore JB, Barr RG, Rosen BR. Proton NMR imaging of cerebral blood flow using $H_2{}^{17}O$. Magn Reson Med. 1991; 22:154–158. [PubMed: 1798389]
33. Kwong KK, Xiong J, Kuan WP, Cheng HM. Measurement of water movement in the rabbit eye in vivo using $H_2{}^{17}O$. Magn Reson Med. 1991; 22:443–450. [PubMed: 1812378]
34. Mateescu GD, Cabrera ME. In vivo ^{17}O magnetic resonance spectroscopy. Determination of temperature effects on metabolic rates (Q10 factor). Adv Exp Med Biol. 1997; 411:585–590. [PubMed: 9269476]
35. Mateescu GD, LaManna JC, Lust WD, Mars LM, Tseng J. Oxygen-17 magnetic resonance: in vivo detection of nascent mitochondrial water in animals breathing $^{17}O_2$ enriched air. Proc Inter Soc Magn Reson Med. 1991:1031.

36. Arai T, Nakao S, Mori K, Ishimori K, Morishima I, Miyazawa T, Fritz-Zieroth B. Cerebral oxygen utilization analyzed by the use of oxygen-17 and its nuclear magnetic resonance. Biochem Biophys Res Commun. 1990; 169:153–158. [PubMed: 2350339]
37. Pekar J, Sinnwell T, Ligeti L, Chesnick AS, Frank JA, McLaughlin AC. Simultaneous measurement of cerebral oxygen consumption and blood flow using ^{17}O and ^{19}F magnetic resonance imaging. J Cereb Blood Flow Metab. 1995; 15:312–320. [PubMed: 7860664]
38. Fiat D, Dolinsek J, Hankiewicz J, Dujovny M, Ausman J. Determination of regional cerebral oxygen consumption in the human: ^{17}O natural abundance cerebral magnetic resonance imaging and spectroscopy in a whole body system. Neurol Res. 1993; 15:237–248. [PubMed: 8105403]
39. Fiat D, Kang S. Determination of the rate of cerebral oxygen consumption and regional cerebral blood flow by non-invasive ^{17}O in vivo NMR spectroscopy and magnetic resonance imaging: Part 1. Theory and data analysis methods. Neurol Res. 1992; 14:303–311. [PubMed: 1360624]
40. Fiat D, Kang S. Determination of the rate of cerebral oxygen consumption and regional cerebral blood flow by non-invasive ^{17}O in vivo NMR spectroscopy and magnetic resonance imaging. Part 2. Determination of $CMRO_2$ for the rat by ^{17}O NMR, and $CMRO_2$,rCBF and the partition coefficient for the cat by ^{17}O MRI. Neurol Res. 1993; 15:7–22. [PubMed: 8098859]
41. Ronen I, Lee JH, Merkle H, Ugurbil K, Navon G. Imaging $H_2{}^{17}O$ distribution in a phantom and measurement of metabolically produced $H_2{}^{17}O$ in live mice by proton NMR. NMR Biomed. 1997; 10:333–340. [PubMed: 9471124]
42. Ronen I, Merkle H, Ugurbil K, Navon G. Imaging of $H_2{}^{17}O$ distribution in the brain of a live rat by using proton-detected ^{17}O MRI. Proc Natl Acad Sci USA. 1998; 95:12934–12939. [PubMed: 9789018]
43. Ronen I, Navon G. A new method for proton detection of $H_2{}^{17}O$ with potential applications for functional MRI. Magn Reson Med. 1994; 32:789–793. [PubMed: 7869903]
44. Reddy R, Stolpen AH, Charagundla SR, Insko EK, Leigh JS. ^{17}O-decoupled ^{1}H detection using a double-tuned coil. Magn Reson Imaging. 1996; 14:1073–1078. [PubMed: 9070998]
45. Stolpen AH, Reddy R, Leigh JS. ^{17}O-decoupled proton MR spectroscopy and imaging in a tissue model. J Magn Reson. 1997; 125:1–7. [PubMed: 9245354]
46. Charagundla SR, Stolpen AH, Leigh JS, Reddy R. Off-resonance proton T_{1rho} dispersion imaging of ^{17}O-enriched tissue phantoms. Magn Reson Med. 1998; 39:588–595. [PubMed: 9543421]
47. Reddy R, Stolpen AH, Leigh JS. Detection of ^{17}O by proton T_{1rho} dispersion imaging. J Magn Reson B. 1995; 108:276–279. [PubMed: 7670758]
48. Sergeyev NM, Sergeyeva ND, Raynes WT. Isotope Effects on the ^{17}O, ^{1}H Coupling Constant and the ^{17}O-{^{1}H} Nuclear Overhauser Effect in Water. J Magn Reson. 1999; 137:311–315. [PubMed: 10089164]
49. Abragam, A. The Principles of Nuclear Magnetism. Oxford University Press; London: 1961.
50. Glasel JA. A study ofwater in biological systems of O-17 magnetic resonance spectroscopy. I. Prliminary studies and enon hydrates. Proc Natl Acad Sci USA. 1966; 55:479–485. [PubMed: 5222013]
51. Meiboom S. NMR study of the proton transfer in water. J Chem Phys. 1961; 34:375–388.
52. Zhu XH, Merkle H, Kwag JH, Ugurbil K, Chen W. ^{17}O relaxation time and NMR sensitivity of cerebral water and their field dependence. Magn Reson Med. 2001; 45:543–549. [PubMed: 11283979]
53. Lauterwein J, Lukacs G, Poupon MF, Schumacher M. Oxygen-17 relaxation times in the blood sera of rats with various cancers. Can a systemic effect be detected? Physiological Chemistry and Physics and Medical NMR. 1986; 18:137–140. [PubMed: 3809262]
54. Thelwall PE, Blackband SJ, Chen W. Field dependence of ^{17}O T_1, T_2 and SNR - in vitro and in vivo studies at 4.7, 11 and 17.6 Tesla. Proc Intl Soc Mag Reson Med. 2003:504.
55. Ernst, RR.; Bodenhausen, G.; Wokaun, A. Principles of Nuclear Magnetic Resonance in One and Two Dimensions. Oxford University Press; New York: 1987.
56. Hoult DI, Richards RE. The signal-to-noise ratio of the nuclear magnetic resonance experiment. J Magn Reson. 1976; 24:71–85.

57. Wang Z, Wang DJ, Noyszewski EA, Bogdan AR, Haselgrove JC, Reddy R, Zimmerman RA, Leigh JS. Sensitivity of in vivo MRS of the N-d proton in proximal histidine of deoxymyoglobin. Magn Reson Med. 1992; 27:362–367. [PubMed: 1334205]
58. Wen H, Chesnick AS, Balaban RS. The design and test of a new volume coil for high field imaging. Magn Reson Med. 1994; 32:492–498. [PubMed: 7997115]
59. Cassoly R. Interaction of hemoglobin with the red blood cell membrane. A saturation transfer electron paramagnetic resonance study. Biochim Biophys Acta. 1982; 689:203–209. [PubMed: 6288095]
60. Zhang N, Zhu XH, Lei H, Ugurbil K, Chen W. Simplified methods for calculating cerebral metabolic rate of oxygen based on ^{17}O magnetic resonance spectroscopic imaging measurement during a short $^{17}O_2$ inhalation. J Cereb Blood Flow Metab. 2004; 24:840–848. [PubMed: 15362714]
61. Yeung HN, Lent AH. Proton transverse relaxation rate of ^{17}O-enriched water. Magn Reson Med. 1987; 5:87–92. [PubMed: 2821341]
62. Mateescu, GD.; Yvars, GM.; Pazara, DI.; Alldridge, NA.; LaManna, JC.; Lust, WD.; Mattingly, M.; Kuhn, W. Combined oxygen-17/proton magnetic resonance microscopy in plants, animals and materials: present status and potential. In: Bailie, TA.; Jones, JR., editors. Synthesis and applications of isotopically labelled compounds. Elsevier; Amsterdam: 1989. p. 499-508.
63. Arai T, Gupte PM, Lasker SE, Del Guercio LR, Mori K. Method for the detection of tissue metabolite ($H_2{}^{17}O$) in brain by proton magnetic resonance imaging. Crit Care Med. 1989; 17:1333–1334. [PubMed: 2556246]
64. de Crespigny AJ, D'Arceuil HE, Engelhorn T, Moseley ME. MRI of focal cerebral ischemia using ^{17}O-labeled water. Magn Reson Med. 2000; 43:876–883. [PubMed: 10861883]
65. Rizi RR, Charagundla SR, Song HK, Reddy R, Stolpen AH, Schnall MD, Leigh JS. Proton T1rho-dispersion imaging of rodent brain at 1.9 T. J Magn Reson Imaging. 1998; 8:1090–1096. [PubMed: 9786147]
66. Makela HI, Grohn OH, Kettunen MI, Kauppinen RA. Proton exchange as a relaxation mechanism for T_1 in the rotating frame in native and immobilized protein solutions. Biochem Biophys Res Commun. 2001; 289:813–818. [PubMed: 11735118]
67. Grohn OHJ, Kettunen MI, Makela HI, Penttonen M, Pitkanen A, Lukkarinen JA, Kauppinen RA. Early detection of irreversible cerebral ischemia in the rat using dispersion of the magnetic resonance imaging relaxation time, T_{1rho}. J Cereb Blood Flow Metab. 2000; 20:1457–1466. [PubMed: 11043908]
68. Kettunen MI, Grohn OH, Penttonen M, Kauppinen RA. Cerebral T_{1rho} relaxation time increases immediately upon global ischemia in the rat independently of blood glucose and anoxic depolarization. Magn Reson Med. 2001; 46:565–572. [PubMed: 11550250]
69. Tailor DR, Roy A, Regatte RR, Charagundla SR, McLaughlin AC, Leigh JS, Reddy R. Indirect ^{17}O-magnetic resonance imaging of cerebral blood flow in the rat. Magn Reson Med. 2003; 49:479–487. [PubMed: 12594750]
70. Tailor DR, Poptani H, Glickson JD, Leigh JS, Reddy R. High-resolution assessment of blood flow in murine RIF-1 tumors by monitoring uptake of $H_2{}^{17}O$ with proton T(1rho)-weighted imaging. Magn Reson Med. 2003; 49:1–6. [PubMed: 12509813]
71. Mellon EA, Beesam RS, Baumgardner JE, Borthakur A, Witschey WR 2nd, Reddy R. Estimation of the regional cerebral metabolic rate of oxygen consumption with proton detected ^{17}O MRI during precision $^{17}O_2$ inhalation in swine. J Neurosci Methods. 2009; 179:29–39. [PubMed: 19428508]
72. Mellon EA, Beesam RS, Elliott MA, Reddy R. Mapping of cerebral oxidative metabolism with MRI. Proc Natl Acad Sci USA. 2010; 107:11787–11792. [PubMed: 20547874]
73. Mellon EA, Beesam RS, Kasam M, Baumgardner JE, Borthakur A, Witschey WR Jr, Reddy R. Single shot T_{1rho} magnetic resonance imaging of metabolically generated water in vivo. Adv Exp Med Biol. 2009; 645:279–286. [PubMed: 19227483]
74. Kety SS, Schmidt CF. The nitrous oxide method for the quantitative determination of cerebral blood flow in man; theory, rocedure and normal values. J Clin Invest. 1948; 27:476–483.

75. Zhu XH, Zhang Y, Tian RX, Lei H, Zhang N, Zhang X, Merkle H, Ugurbil K, Chen W. Development of ^{17}O NMR approach for fast imaging of cerebral metabolic rate of oxygen in rat brain at high field. Proc Natl Acad Sci USA. 2002; 99:13194–13199. [PubMed: 12242341]
76. Fiat D, Ligeti L, Lyon RC, Ruttner Z, Pekar J, Moonen CT, McLaughlin AC. In vivo ^{17}O NMR study of rat brain during $^{17}O_2$ inhalation. Magn Reson Med. 1992; 24:370–374. [PubMed: 1569875]
77. Herscovitch A, Raichle ME. What is the correct value for the brain-blood partition coefficient for water? J Cereb Blood Flow Metab. 1985; 5:65–69. [PubMed: 3871783]
78. Herscovitch P, Raichle ME, Kilbourn MR, Welch MJ. Positron emission tomographic measurement of cerebral blood flow and permeability-surface area product of water using [^{15}O]water and [^{11}C]butanol. J Cereb Blood Flow Metab. 1987; 7:527–542. [PubMed: 3498732]
79. Zhang X, Zhu XH, Tian R, Zhang Y, Merkle H, Chen W. Measurement of arterial input function of ^{17}O water tracer in rat carotid artery by using a region-defined (REDE) implanted vascular RF coil. Magma. 2003; 16:77–85. [PubMed: 12845538]
80. Hyder F, Kennan RP, Kida I, Mason GF, Behar KL, Rothman D. Dependence of oxygen delivery on blood flow in rat brain: a 7 tesla nuclear magnetic resonance study. J Cereb Blood Flow Metab. 2000; 20:485–498. [PubMed: 10724113]
81. Nakao Y, Itoh Y, Kuang TY, Cook M, Jehle J, Sokoloff L. Effects of anesthesia on functional activation of cerebral blood flow and metabolism. Proc Natl Acad Sci USA. 2001; 98:7593–7598. [PubMed: 11390971]
82. Zhu XH, Zhang X, Zhang N, Zhang Y, Strupp J, Ugurbil K, Chen W. High-field ^{17}O Study of 3D $CMRO_2$ Imaging in human visual cortex. Proc Intl Soc Mag Reson Med. 2006:409.
83. Atkinson IC, Thulborn KR. Feasibility of mapping the tissue mass corrected bioscale of cerebral metabolic rate of oxygen consumption using 17-oxygen and 23-sodium MR imaging in a human brain at 9.4 T. Neuroimage. 2010; 51:723–733. [PubMed: 20188194]
84. Lu A, Atkinson IC, Claiborne TC, Damen FC, Thulborn KR. Quantitative sodium imaging with a flexible twisted projection pulse sequence. Magn Reson Med. 2010; 63:1583–1593. [PubMed: 20512862]
85. Nagel AM, Laun FB, Weber MA, Matthies C, Semmler W, Schad LR. Sodium MRI using a density-adapted 3D radial acquisition technique. Magn Reson Med. 2009; 62:1565–1573. [PubMed: 19859915]
86. Brown TR, Kincaid BM, Ugurbil K. NMR chemical shift imaging in three dimensions. Proc Natl Acad Sci USA. 1982; 79:3523–3526. [PubMed: 6954498]
87. Hu, X.; Chen, W.; Patel, M.; Ugurbil, K. Chemical Shift Imaging: An introduction to its theory and practice. In: Bronzino, JD., editor. Biomedical Engineering Handbook. CRC; 1995. p. 1036-1045.
88. Zhu XH, Zhang Y, Zhang N, Ugurbil K, Chen W. Noninvasive and three-dimensional imaging of $CMRO_2$ in rats at 9.4 T: reproducibility test and normothermia/hypothermia comparison study. J Cereb Blood Flow Metab. 2007; 27:1225–1234. [PubMed: 17133228]
89. Erecinska M, Thoresen M, Silver IA. Effects of hypothermia on energy metabolism in Mammalian central nervous system. J Cereb Blood Flow Metab. 2003; 23:513–530. [PubMed: 12771566]
90. Siesjo, BK. Brain energy metabolism. Wiley; New York: 1978.
91. Kety SS, Schmidt CF. The determination of cerebral blood flow in man by the use of nitrous oxide in low concentrations. Am J Physiol. 1945; 143:53–66.
92. Wiesner HM, Balla DZ, Pohmann R, Chen W, Ugurbil K, Uludag K. ^{17}O T_1/T_2* tissue-relaxation rates with anatomical contrast in the rat brain at 16.4 T. Proc Intl Soc Mag Reson Med. 2009:353.
93. Zhu XH, Zhang N, Zhang Y, Ugurbil K, Chen W. New insights into central roles of cerebral oxygen metabolism in the resting and stimulus-evoked brain. J Cereb Blood Flow Metab. 2009; 29:10–18. [PubMed: 18781163]
94. Zhu XH, Lei H, Zhang Y, Zhang XL, Zhang N, Ugurbil K, Chen W. Evidence of limited permeation of metabolic water in rat brain observed by ^{17}O magnetic resonance spectroscopic imaging and its implications. Proc Intl Soc Mag Reson Med. 2002:1094.
95. Fiat D, Hankiewicz J, Liu S, Trbovic S, Brint S. ^{17}O magnetic resonance imaging of the human brain. Neurol Res. 2004; 26:803–808. [PubMed: 15727263]

96. Hoffmann S, Begovatz P, Nagel A, Umathum R, Bock M. In vivo Oxygen-17 (^{17}O) MRI at 7 Tesla. Proc Intl Soc Mag Reson Med. 2010:724.

97. Ogawa S, Lee T-M, Kay AR, Tank DW. Brain magnetic resonance imaging with contrast dependent on blood oxygenation. Proc Natl Acad Sci USA. 1990; 87:9868–9872. [PubMed: 2124706]

98. Bandettini PA, Wong EC, Hinks RS, Tikofsky RS, Hyde JS. Time course EPI of human brain function during task activation. Magn Reson Med. 1992; 25:390–397. [PubMed: 1614324]

99. Kwong KK, Belliveau JW, Chesler DA, Goldberg IE, Weisskoff RM, Poncelet BP, Kennedy DN, Hoppel BE, Cohen MS, Turner R, Cheng HM, Brady TJ, Rosen BR. Dynamic magnetic resonance imaging of human brain activity during primary sensory stimulation. Proc Natl Acad Sci USA. 1992; 89:5675–5679. [PubMed: 1608978]

100. Ogawa S, Tank DW, Menon R, Ellermann JM, Kim SG, Merkle H, Ugurbil K. Intrinsic signal changes accompanying sensory stimulation: functional brain mapping with magnetic resonance imaging. Proc Natl Acad Sci USA. 1992; 89:5951–5955. [PubMed: 1631079]

101. Ogawa S, Menon RS, Tank DW, Kim SG, Merkle H, Ellermann JM, Ugurbil K. Functional brain mapping by blood oxygenation level-dependent contrast magnetic resonance imaging. A comparison of signal characteristics with a biophysical model. Biophys J. 1993; 64:803–812. [PubMed: 8386018]

102. Buxton RB. Interpreting oxygenation-based neuroimaging signals: the importance and the challenge of understanding brain oxygen metabolism. Front Neuroenergetics. :2–8.

103. Zhu XH, Zhang Y, Chen W. Simultaneous and Ultrafast Monitoring of $CMRO_2$, CBF and pO_2 Changes in Response to Acute Global Ischemia in Rat Brain. Proc Intl Soc Mag Reson Med. 2007:2393.

104. Zhu XH, Zhang Y, Wiesner H, Ugurbil K, Chen W. Estimation of CBF Based on the Metabolic $H_2{}^{17}O$ Decay Rate in $CMRO_2$ Measurement Using *In Vivo* ^{17}O MR Approach. Proc Intl Soc Mag Reson Med. 2010:716.

105. Zhu XH, Zhang Y, Chen W. *In Vivo* ^{17}O MRS Imaging for Assessing Myocardial Oxygen Metabolism in Rat Heart at 9.4T. Proc Intl Soc Mag Reson Med. 2010:172.

Highlights

- This article reviews the developments of *in vivo* ^{17}O NMR imaging in brain research.
- *In vivo* ^{17}O NMR imaging has improved significantly at high/ultrahigh field.
- *In vivo* ^{17}O NMR can noninvasively image brain oxygen metabolism and perfusion.
- *In vivo* ^{17}O NMR is useful for mapping the functional change in oxygen metabolism.
- *In vivo* ^{17}O NMR imaging could potentially be used for human and clinic applications.

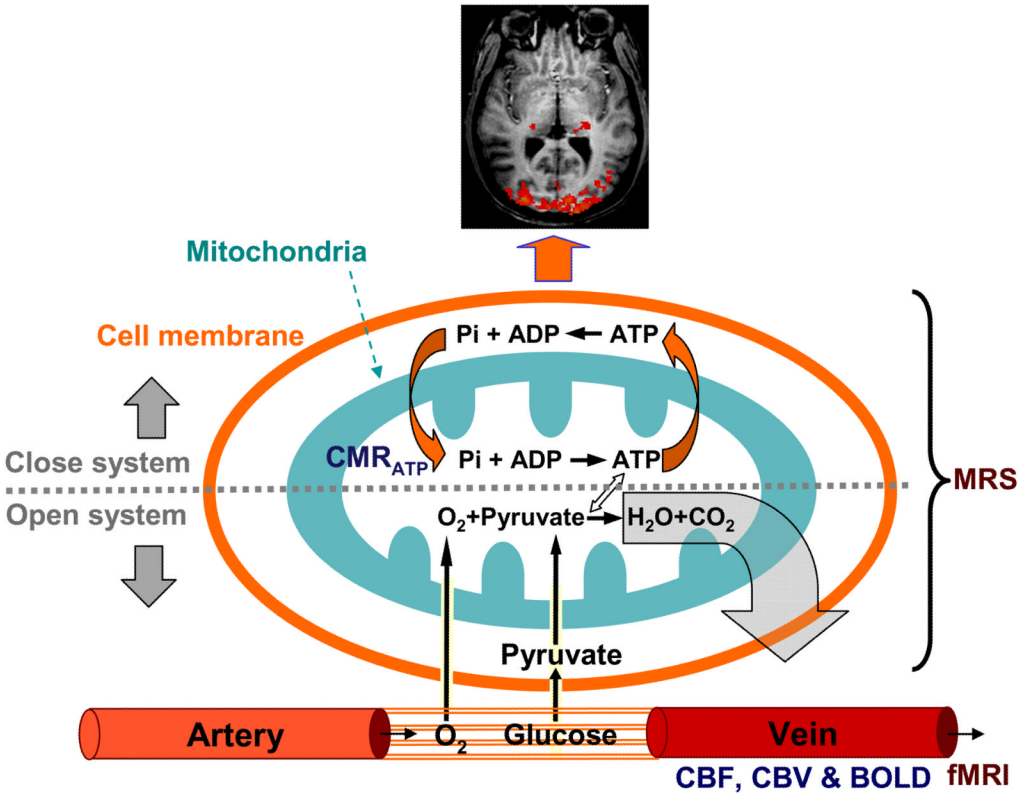

Fig. 1.

Key metabolic processes occur in various sub-cellular compartments including both mitochondria and cytosol spaces and the associated vascular or hemodynamic events of the brain.

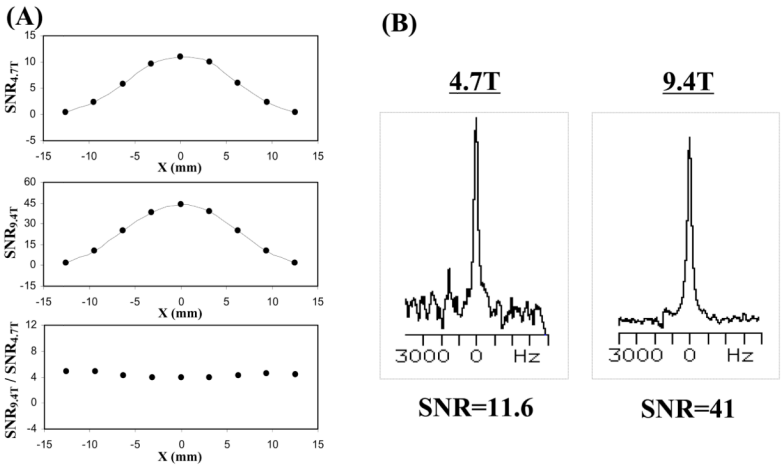

Fig. 2.

(A) One-dimensional SNR profiles of ^{17}O-water signal in the rat brain at 4.7T and 9.4T, and the SNR ratio between 9.4T and 4.7T; (B) Single voxel ^{17}O-MR spectrum of $H_2{}^{17}O$ signal obtained from rat brain at 4.7T and 9.4T, respectively (total acquisition time of 15 s, and nominal voxel size of 16 μl. Adapted from *Zhu et al. MRM 2001; 45: 543–549.*

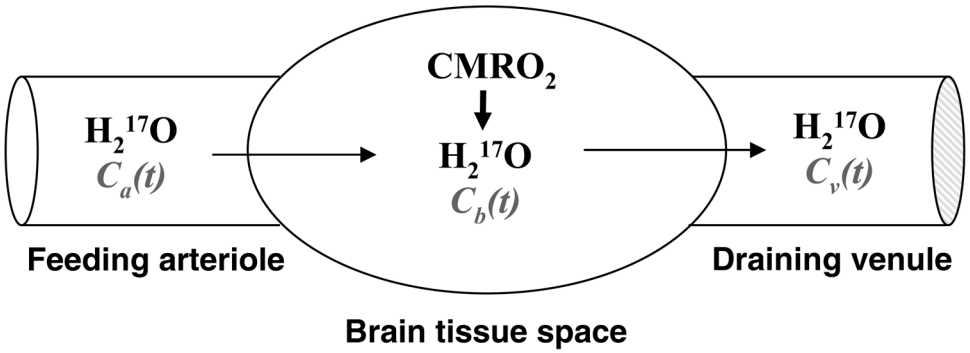

Fig. 3.

Schematic illustration of a "complete model" describing three parallel processes of the ^{17}O-labeled metabolic water ($H_2{}^{17}O$) occurring in the brain when the ^{17}O-labeled oxygen gas molecules are introduced via an inhalation. In this model, only the metabolic $H_2{}^{17}O$ is considered because the ^{17}O-labeled O_2 is invisible by *in vivo* ^{17}O NMR. $C_a(t)$, $C_b(t)$ and $C_v(t)$ stand for the $H_2{}^{17}O$ concentration in arteriole, brain tissue and venule, respectively, as a function of the $^{17}O_2$ inhalation time.

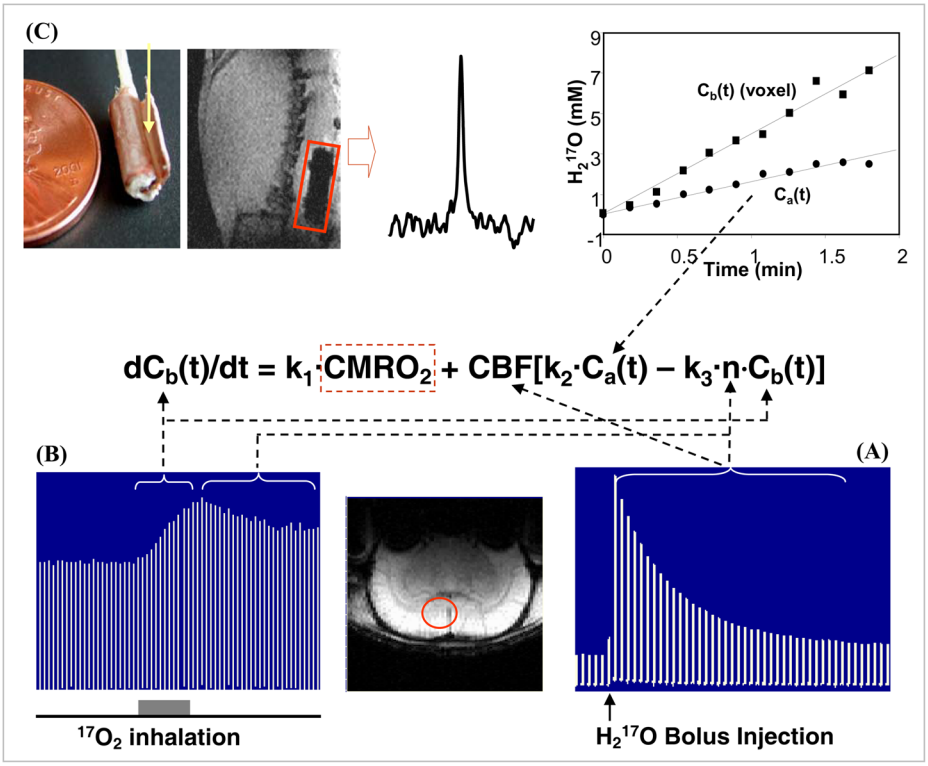

Fig. 4.

Schematic diagram showing the multiple *in vivo* ^{17}O measurements at 9.4T for determining $CMRO_2$ using the complete model according to the mass balance equation of Eq. [7] which links $C_b(t)$, $C_a(t)$, CBF and *n* with $CMRO_2$. To simplify the equation, three known constants of $2\alpha f_1$, mf_2 and m/λ used in Eq. [7] are replaced by k_1, k_2 and k_3, respectively. (A) Stacked plot of the ^{17}O spectra of cerebral $H_2{}^{17}O$ tracer from one representative voxel as indicated by the circle in the anatomical brain image (low center insert). The spectra were acquired before and after a bolus injection of $H_2{}^{17}O$ for CBF measurements. (B) Stacked plot of the ^{17}O spectra of the metabolic $H_2{}^{17}O$ from the same voxel acquired before (natural abundance), during (as indicated by the gray bar under the stacked plot) and after a 2-minute $^{17}O_2$ inhalation. (C) Measurement of $C_a(t)$ by using an implanted ^{17}O RF coil (the left insert). The middle insert illustrates an ^{17}O spectrum of natural abundance $H_2{}^{17}O$ obtained from the rat carotid artery blood with the implanted coil before $^{17}O_2$ inhalation. The right insert shows the time course of $C_a(t)$ (circle symbol) and $C_b(t)$ from a representative 3D ^{17}O CSI voxel (square symbol) in the same rat during the $^{17}O_2$ inhalation. Finally, the ratio between the ^{17}O signal decay detected after a bolus injection of $H_2{}^{17}O$ (see Fig. 4A) versus the ^{17}O signal decay detected after the cessation of $^{17}O_2$ inhalation (see Fig. 4B) gives the constant of *n*. Adapted from *Zhu et. al. PNAS 2002; 99: 13194–13199.*

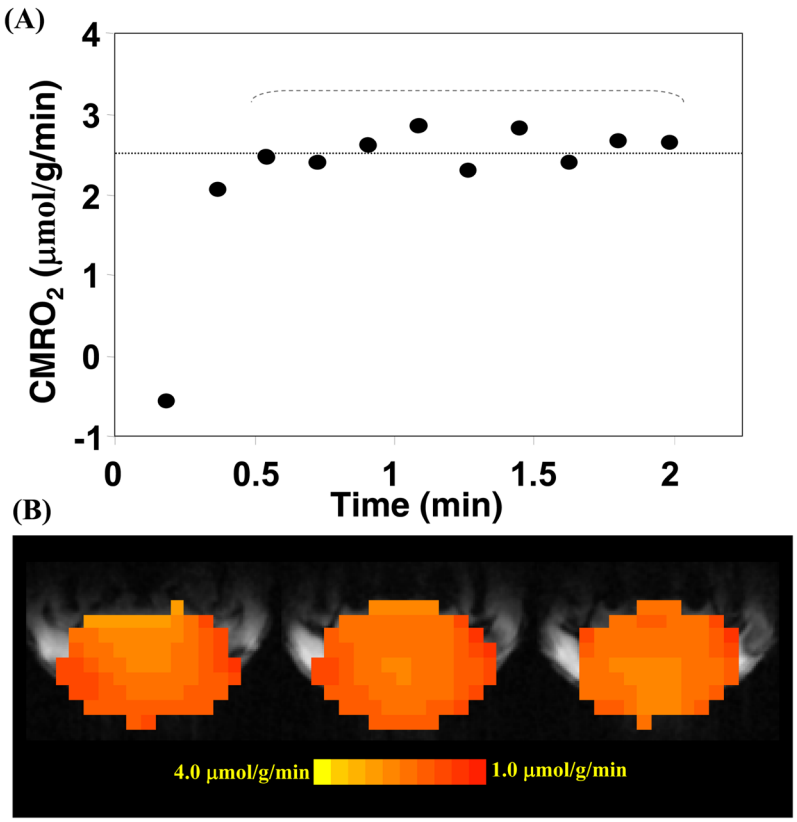

Fig. 5.

(A) Plot of the calculated $CMRO_2$ values using the complete model as described by Eq. [8] as a function of $^{17}O_2$ inhalation time. (B) Three-dimensional coronal $CMRO_2$ images of rat brain measured by *in vivo* ^{17}O MRS approach during a 2-minute $^{17}O_2$ inhalation at 9.4 Tesla. Adapted from *Zhu et. al. PNAS 2002; 99: 13194–13199.*

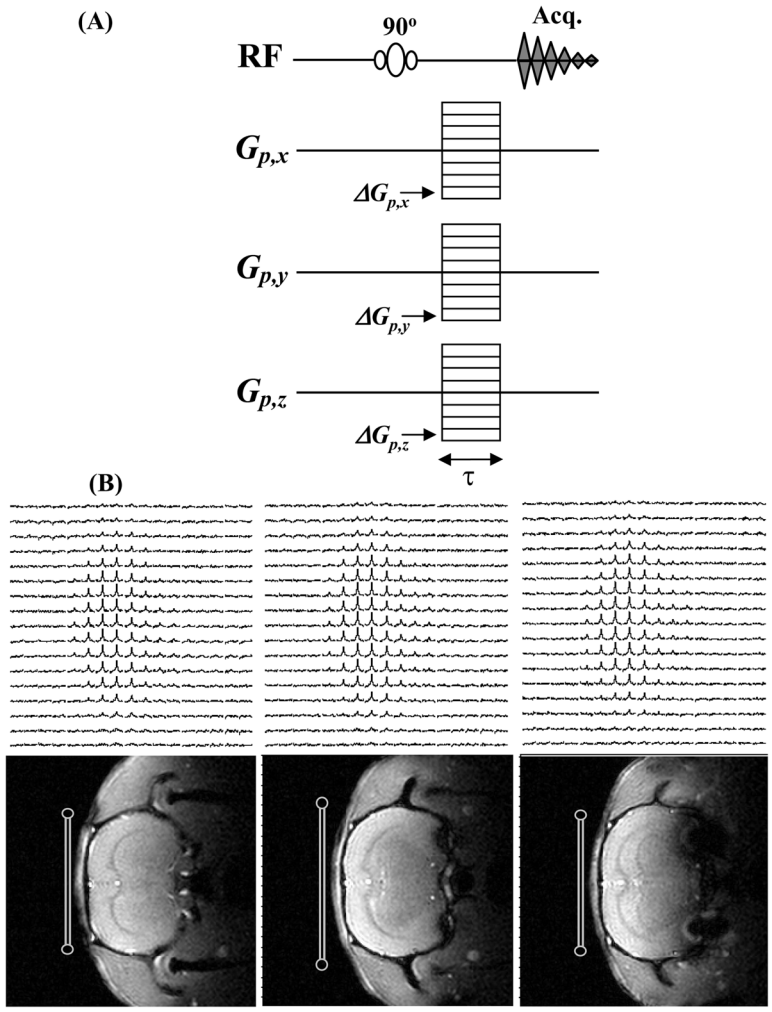

Fig. 6.

(A) 3D chemical shift imaging sequence; and (B) 3D ^{17}O CSI data of natural abundance $H_2{}^{17}O$ (top row) and corresponding ^{1}H anatomical images (bottom row) of rat brain acquired at 9.4T. The RF ^{17}O surface coil positions and cross sections are indicated in the images.

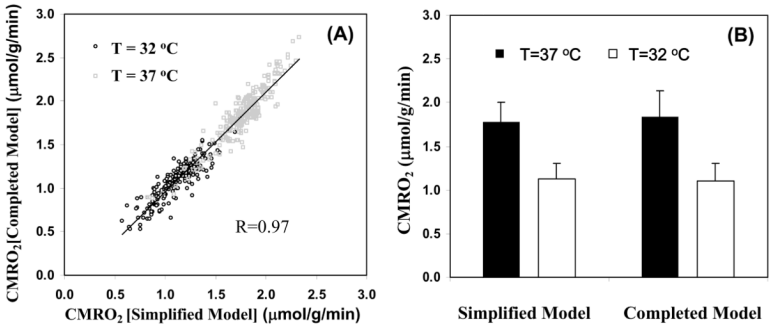

Fig. 7.

(A) Voxel based $CMRO_2$ calculation and comparison using the completed and simplified models from a representative rat (total voxel number used was 224 for 32°C and 254 for 37°C, voxel size = 75μl). (B) Averaged $CMRO_2$ values in the same rat brain at normothermia (37°C) and hypothermia (32°C) condition, calculated with simplified and completed model, respectively. Adapted from *Zhu et. al. JCBFM 2007; 27(6): 1225–1234.*

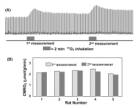

Fig. 8.

(A) Stacked plots of $H_2{}^{17}O$ spectra from a representative voxel of 3D ^{17}O MRSI data acquired before, during and after two consecutive 2-min $^{17}O_2$ inhalations in a rat brain at 9.4T. (B) The comparison results between two repeated $CMRO_2$ measurements in five rat brains. Adapted from *Zhu et. al. JCBFM 2007; 27(6): 1225–1234.*

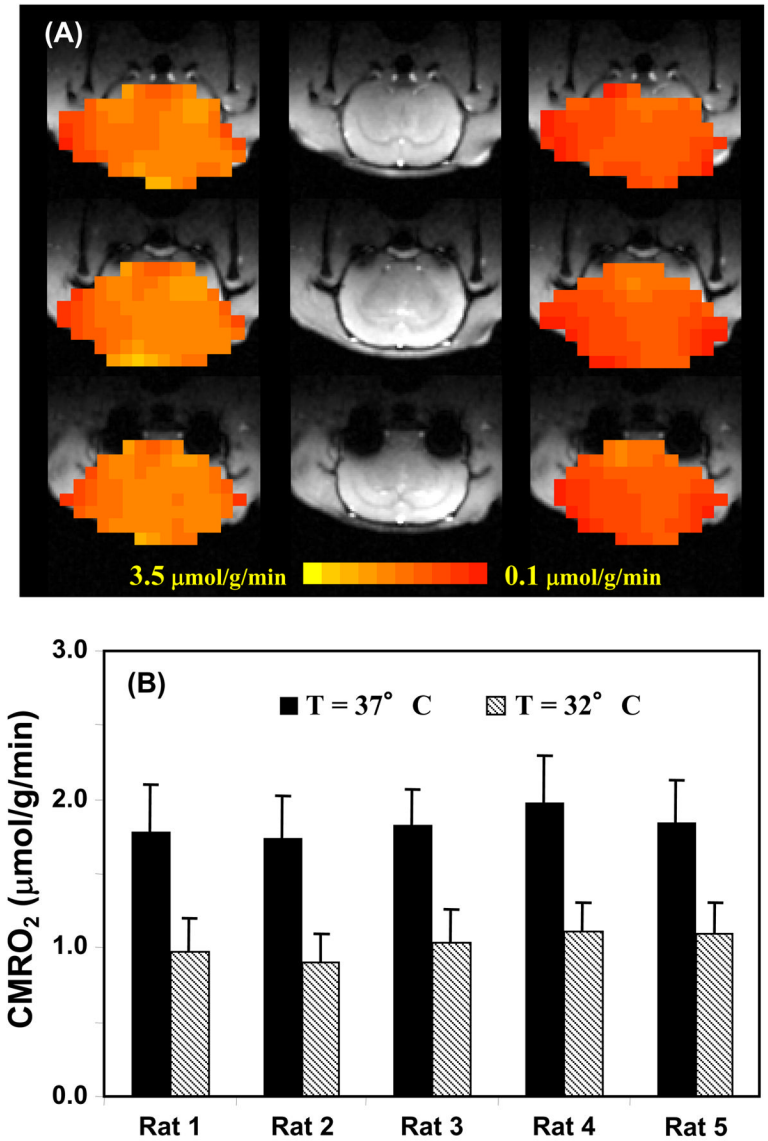

FIG. 9.

(A) Anatomic images (middle column) of a representative rat brain and the corresponding multi-slices $CMRO_2$ maps obtained using 3D ^{17}O-CSI approach at 9.4T under normothermia (left column) and hypothermia (right column) conditions, (B) Summary of $CMRO_2$ results measured at normothermia and hypothermia conditions (n=5). Adapted from *Zhu et. al. JCBFM 2007; 27(6): 1225–1234.*

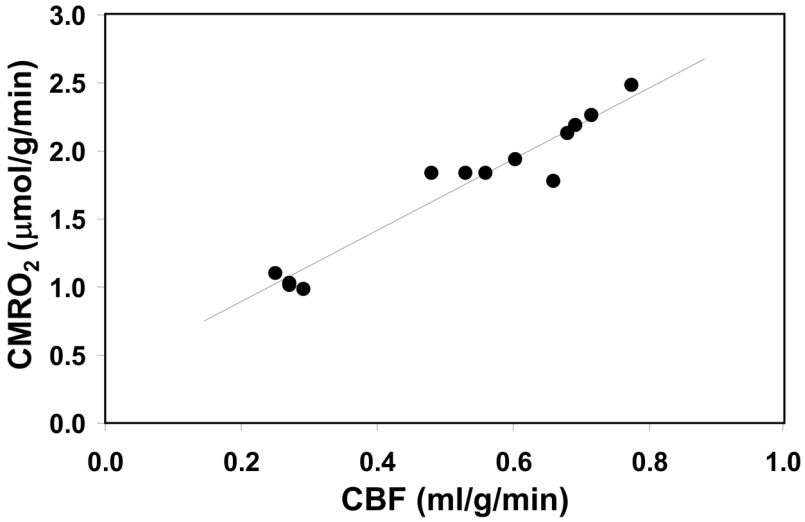

Fig. 10.

Correlation of CBF and $CMRO_2$ values in rat brains anesthetized with a-chloralose at brain temperature range of 32–37°C. The linear correlation coefficient (R) is 0.97. Adapted from *Zhu et. al. JCBFM 2007; 27(6): 1225–1234.*

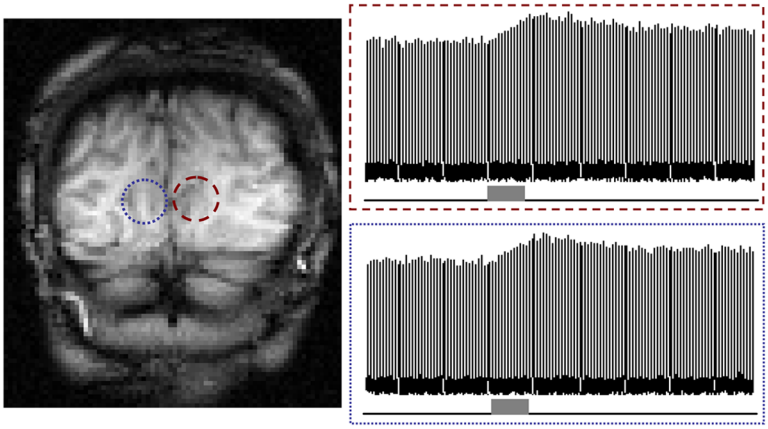

Fig. 11.

Stacked plots of $H_2{}^{17}O$ signal measured by 3D ^{17}O CSI at 7T before (i.e., natural abundance), during and after an 2 min $^{17}O_2$ gas inhalation from two representative voxels in the human visual cortex.

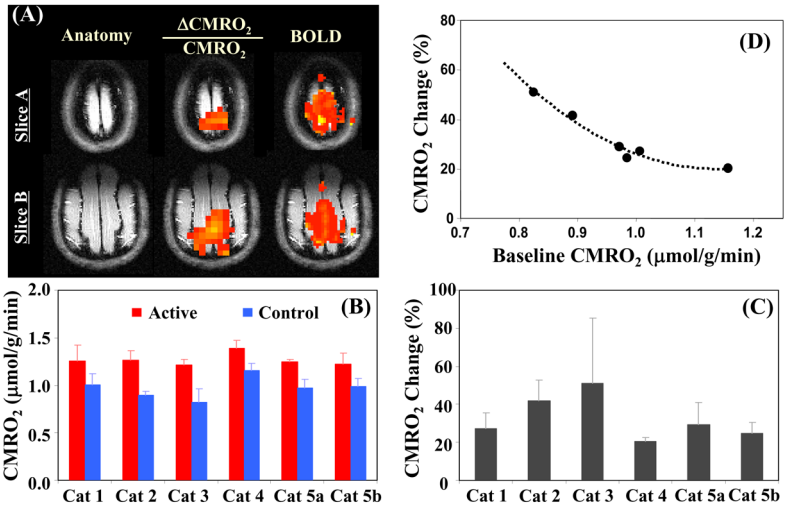

Fig. 12.

(A) Functional maps of BOLD and $CMRO_2$ changes during visual stimulation from a representative cat brain; (B) averaged control (baseline) and activated $CMRO_2$ values; (C) relative $CMRO_2$ changes; and (D) negative correlation between the percent $CMRO_2$ changes and baseline $CMRO_2$ values (n=6). Adapted from *Zhu et. al. JCBFM 2009; 29: 10–18.*

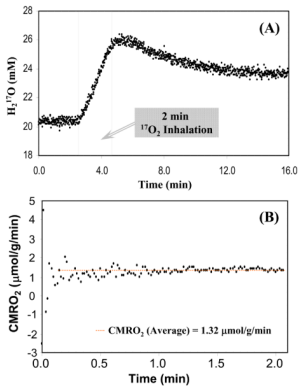

Fig. 13.

Ultra-fast $CMRO_2$ measurement in rat brain at 9.4T: (A) Dynamics of the ^{17}O-water contents in rat brain tissue before, during and after a 2min $^{17}O_2$ gas inhalation obtained with 1 sec temporal resolution; and (B) the $CMRO_2$ values obtained during the inhalation period were quantified using the complete model as described by Eq.[8].

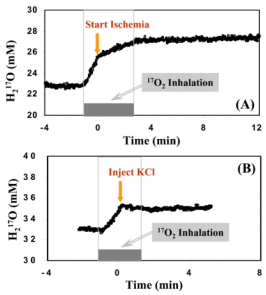

Fig. 14.

Dynamics of the ^{17}O-water contents in rat brain tissue before, during and after short $^{17}O_2$ gas inhalation obtained with ultra-fast $CMRO_2$ measurement approach at 9.4T: (A) forebrain ischemia and (B) KCl injection were performed during the inhalation as indicated by the arrows.

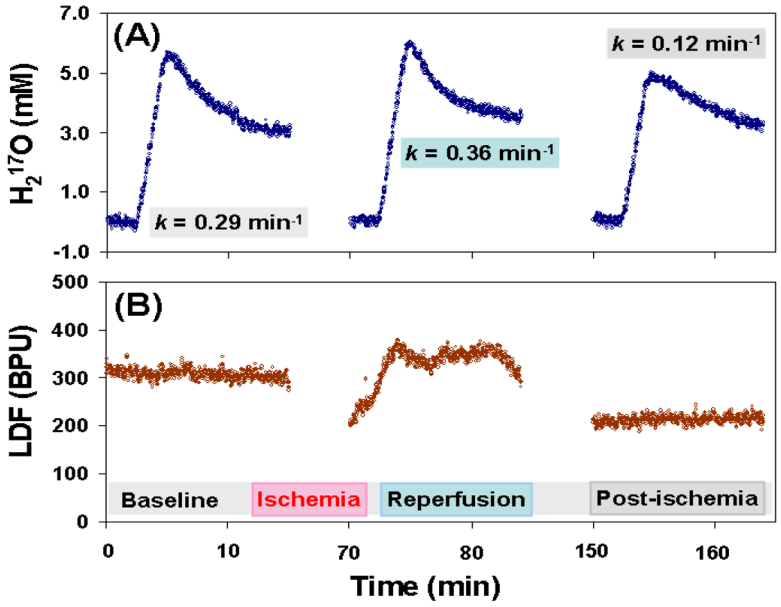

Fig. 15.

Multiple and simultaneous $CMRO_2$ (A) and CBF (B) measurements using ^{17}O-MR approach at 9.4T and Laser Doppler Flow meter (LDF), respectively, in a representative rat brain with global forebrain ischemia preparation. The $H_2{}^{17}O$ decay rates during the baseline, reperfusion and post-ischemia periods were quantified in (A) and they correlate well with the relative CBF changes as shown in (B).